

Ecological mangrove restoration with permeable structures

Monitoring report





Netherlands Enterprise Agency



Document identification

Programme name *Building with Nature Indonesia - Securing Eroding Delta Coastlines*

Result Monitoring of the Permeable Structures

Authors Amrit, Cado, Floris van Rees, Miguel de Lucas Pardo, Bregje van Wesenbeeck

Reviewer Peter Herman and Han Winterwerp (Independent)

Date 01/02/2021

Dissemination level

PU Public

Version

Date

3.0

01-02-2021

Project statement

This report was written in the context of the **Building with Nature Indonesia Programme - Securing Eroding Delta Coastlines** by [Ecoshape](#), [Wetlands International](#), the Indonesian Ministry of Marine Affairs and Fisheries (MMAF), and the Indonesian Ministry of Public Works and Human Settlement (PU), in partnership with [Witteveen+Bos](#), [Deltares](#), [Wageningen University & Research Centre](#), [UNESCO-IHE](#), [Blue Forests](#), and [Von Lieberman](#), with support from the [Diponegoro University](#), and local communities.

“Building with Nature Indonesia” is supported by the Dutch Sustainable Water Fund (Netherlands Enterprise Agency), the German Federal Ministry for the Environment, Nature Conservation and Nuclear Safety (BMU) as part of the International Climate Initiative (IKI), Waterloo Foundation, Otter Foundation, Topconsortia for Knowledge and Innovation, and Mangroves for the Future.

Disclaimer

Project partners are committed to drive the current Building with Nature innovation trajectory, by demonstrating the approach in a case study site in Demak. Successful implementation requires in-depth system understanding, extensive stakeholder engagement, and adaptive management on the basis of monitoring and evaluation. We stimulate and support upscaling of the approach by disseminating knowledge, lessons learned and implementation guidance. Stakeholders interested to replicate our approach are strongly recommended to adhere to this guidance and bear full responsibility for the success and sustainability of the approach. The picture on the title page was taken during one of the many field visits over the course of a 4 year monitoring period (2015 – 2019).

Effectiveness of a Nature based Solution

Monitoring of Ecological mangrove restoration by use of permeable structures

Client	Wetlands International and Ecoshape
Contact	Femke Tonneijck en Fokko van der Groot
Reference	
Keywords	Mangrove restoration, Permeable structures, Monitoring, Building with Nature

Document control

Version	3.0
Date	03-02-2021
Project nr.	1220476-000
Document ID	1220476-000-ZKS-0010
Pages	51
Status	final

Doc. version	Author	Reviewer	Approver	Publish
1.0	Amrit Cado Miguel de Lucas Pardo Bregje van Wesenbeeck	Peter Herman		July 2020
2.0	Amrit Cado Floris van Rees Miguel de Lucas Pardo Bregje van Wesenbeeck	Peter Herman Han Winterwerp	Toon Segeren	November 2020
3.0	Amrit Cado Bregje van Wesenbeeck	Peter Herman Han Winterwerp	Toon Segeren	February 2021

Summary

In this study, the use of permeable structures was tested as a means of mangrove habitat restoration in Demak, Indonesia. Structures are designed to attenuate waves and create still water conditions for trapping sediment, hereby creating suitable habitat for natural mangrove colonization and revert eroding coastlines into accreting coastlines. This project was part of an overarching Building with Nature (BwN) Indonesia programme aiming at mitigation of coastal erosion in Demak through construction of permeable structures and at improving local livelihoods.

Over the course of 4 years the effectiveness of permeable structures for mangrove restoration were monitored. The current study aims at answering the following questions for the situation in Demak.

1. Are permeable structures effective in trapping sediment?
2. Can mangrove colonization take place behind the permeable structures?
3. Do mangroves colonize and develop into healthy mangrove forest behind the structures?

Globally 20% of all mangroves is lost with excesses in South East Asia where one third of the mangrove habitat already disappeared. Mangrove loss commenced in the beginning of last century and is still on-going. Unabated population growth led to conversion of mangrove habitat into aqua- and agriculture. High rates of subsidence, caused by groundwater extraction, and reduction in sediment supply, caused by dams and embankments, is disrupting the sediment balance in mangrove ecosystems. As a result, mangroves are no longer able to cope with sea level rise and against the backdrop of climate change this problem will only worsen.

Over the last few decades districts along the north coast of Java have experienced severe coastal inundation and erosion events. One such area is Demak, where communities experienced coastal retreat over 2 km. Hard structures such as seawalls, worsen the problem by aggravating erosion due to interference with sediment flows and amplifying wave heights and erosive forces. Thus, there is an urgency for effective methods of mangrove restoration. However, many restoration efforts failed to recognize the underlying reasons of mangrove decline, i.e.: unsuitable hydrological conditions, longer submergence times, increased wave impact and unfavourable soil properties (pH, bulk density, nutrients, etc.). The common practice of planting mangroves showed low rates of success by not addressing the root cause. Understanding the system and modifying abiotic conditions to become suitable for mangrove recovery may cause mangroves to return without active planting.

The use of brushwood to restore coastal habitat is centuries old. Along the German and Dutch Wadden Sea, land reclamation was done using a similar design as in Indonesia and Vietnam. Structures in the current study are approximately 100 meters long and have an opening of approximately 10 m in the middle. Initially, permeable structures were constructed with local materials, such as brushwood and bamboo. This method was reported to be successful in Vietnam, where within three years mangrove recruitment was enhanced. Most recent designs also used PVC poles that were filled with concrete. The spatial design aimed at facilitating a gradual seaward advancement of the coastline. Structures are placed perpendicular on the prevailing wave direction and not further than 100 metres from the initial coastline, to prevent wave set-up behind the structure. Once the mangroves colonized the sheltered area behind the structure, a new structure was placed further seaward. Monitoring took place at 19 permeable structures and at 80 different locations. Sediment bed level was monitored monthly on the seaward and the landward side of the structure, where seaward points were used as controls for natural bed level dynamics. Monitoring was done by using a 2-meter PVC pole that was placed 1 meter into the sediment. Changes in bed level relative to the pole were measured and noted. Mangrove count, size class and mangrove distance from the nearest structure were monitored monthly. Bulk density was measured at different depths and locations twice a year.

Overall, data showed a stark difference in sediment bed level between locations that are sheltered by the structures and the seaward control locations. Areas protected by structures had a 20 – 30 cm higher bed level on average. This difference came about in the first 12 weeks after structure placement. Afterwards the trend plateaued. Total bed level differed significantly between different structures.

Data revealed different trends for different geographic locations which may be driven by differences in exposure to wind and waves. Qualitative inspection of the data showed that degree of exposure is governing variation, i.e. dynamic cheniers in front of structures dampen incoming waves and fringing mangroves can shelter structures. The effect of structures on raising the bed level strongly depended on depth of the structure and the bed with respect to relative sea level with more shallow structures expressing increasing bed levels on average. Furthermore, structures that are placed too far seaward where exposure is high, are less effective at raising sediment bed level. Finally, maintenance of the structures played an important role. During the stormy season, degraded structures lost all accumulated sediment, lowering bed level, and mangroves that might have settled. Although sediment would rapidly return after structures were repaired, the settling and consolidation process completely restarted. Hereby slowing down restoration efforts, as mangroves require dense sediment to withstand wave induced hydraulic drag forces. Mangroves were present in the highly sheltered locations throughout the entire campaign.

Finally, monitoring results were confounded by ongoing subsidence in the area. Field observations on houses and bridges and talks with community members suggest a substantial lowering of the area as a result of subsidence. Expected is that subsidence rates range between 5 – 10 cm per year. With higher water depths, larger waves are formed, causing increasing bed shear stresses, thus enhanced erosion. This may result in newly deposited sediments, being brought into resuspension. Also, subsidence increases the inundation period and wave height, thus lowering bulk density and reducing drainage. All these parameters were altered in an unfavourable manner for settlement and growth of mangroves. Finally, the levels of subsidence also asked for much higher levels of maintenance of permeable structures.

Concluding, permeable structures are considered an effective method for creating favourable conditions for mangroves along coastlines with low to moderate wave impact. These structures represent an adaptive and low-tech measure that can be maintained by coastal communities. In the case that subsidence rates exceed sedimentation rates, permeable structures can at best delay erosive forces that occur locally. To maintain a sustainable coastline, mitigative measures that address the root cause of subsidence must be addressed and implemented.

Contents

Colofon	3	
	Summary	5
1	Introduction	9
2	Materials and Methods	12
2.1	Site description	12
2.2	Permeable Structures	13
2.2.1	Functional design	13
2.2.2	Spatial Design	13
2.2.3	Maintenance	13
2.3	Sediment bed level time series	14
2.3.1	Data collection and field design for sediment bed level time series	14
2.3.2	Statistical analysis of in sediment bed level height	15
2.3.3	Statistical analysis of sediment bed level before and after treatment.	15
2.4	Spatial mapping of sediment bed level in relation to mean sea level	15
2.4.1	Data collection and field design for spatial mapping of sediment bed level	15
2.5	Spatial mapping of Soft mud layer	16
2.5.1	Data collection and field design for spatial mapping of soft mud layer	16
2.5.2	Calculation of soft mud layer	16
2.6	Bulk density measurements	16
2.6.1	Data collection and field design for consolidation	16
2.6.2	Bulk density calculation	17
2.7	Mangrove count data	17
2.7.1	Data collection and field design for mangrove count	17
2.7.2	Temporal and spatial correlation of mangrove data	17
2.8	Software	17
3	Results	18
3.1	State of permeable structures	18
3.2	Sediment bed level results	19
3.2.1	Time series	19
3.2.2	Spatial variability of time series	22
3.2.3	SBL before and after placement of permeable structure	22
3.2.4	Spatial measurements of sediment bed level and Soft mud layer	23
3.2.5	Distance to structure	25
3.3	Mean sea level	26
3.4	Mangrove Count	28
4	Discussion	29
4.1	General	29
4.2	Sediment bed level change	29
4.3	Mangrove Recruitment	30
4.4	Methodological	30
4.5	Subsidence	31
4.6	Variation in spatial characteristics	32
4.7	Conclusion	32
5	References	35
A	Appendix: Locations of PVC measuring poles and permeable structures.	39

B	Appendix: Locations of single measuring event in September of 2019	40
C	The state of permeable structure	41
D	Summary of consolidation analysis	42
D.1	Introduction	42
D.2	Methodology	42
D.2.1	Laboratory tests	42
D.2.2	Field observations	43
D.2.3	Model	43
D.3	Results	44
D.3.1	Input to consolidation model I: laboratory tests with low initial sediment concentration	44
D.3.2	Input to consolidation model II: field measurements	45
D.3.3	In-situ bulk density profiles	46
D.3.4	Model results	46
D.4	Discussion – conclusion	49
D.5	References	50

Mangroves protect coastal communities from waves, erosion and storms (Dahdouh-Guebas et al. 2005; Quartel et al. 2007; Gedan et al. 2011; Montgomery et al. 2018; del Valle et al. 2019). Their complex root structure promotes dissipation of currents and waves, which results in enhanced accretion and reduced erosion of sediment (Carlton 1974, Chen et al., 2018, Brunier et al. 2019). Since mangroves are able to increase soil elevation they can keep up with moderate rates of sea level rise (Borsje et al. 2011, Gedan et al. 2011, Lovelock et al. 2015). Not only are they a natural form of coastal defence but they also act as a carbon sink (Eong 1993; Donato et al. 2011), create fish habitat for economically important fish species (Polidoro et al. 2010) and help prevent salt water intrusion (Bennett and Reynolds 1993). Essentially mangroves create a unique coastal habitat that is in a state of constant flux (Toorman et al. 2018) and contribute to coastal economies and social wellbeing (Gedan et al. 2010).

Over the last 4 decades global trends show a 20% loss of mangrove area (Valiela et al. 2001, Barbier 2016, Friess et al. 2019). In South East Asia these trends are even worse, more than one third of the total mangrove habitat was lost between the 1980s and the 1990s (Spalding 2011). This decline is caused by an ongoing need for natural resources and space, as coastal communities urbanize mangrove habitat and convert it to aquaculture and agriculture (Defries et al. 2010). One of the major issues related to mangrove removal is the consequent coastal erosion, since the mangroves cannot fulfil their protective role any longer (Mazda et al. 2002). Overall, non-climate related anthropogenic stressors account for most mangrove losses. Between 1996-2010 12% of global mangrove cover was lost due to anthropogenic degradation was observed (Thomas et al. 2017). In terms of climate related stressors, by the end of the 2080 sea level rise could cause a decline of 22% of world's coastal wetlands, which includes mangrove habitat (Nicholls et al. 1999). Examples of anthropogenic stressors are subsidence due to groundwater extraction (Gilman et al. 2008, Galloway and Burbey 2011) and reduction of coastal sediment budgets due to the placement of embankments and hydropower plants (Kondolf et al. 2014, Rubin et al. 2015).

Mangrove restoration is urgently needed to reverse mangrove loss and the associated coastal retreat. Most restoration practices focus on planting. Globally, thousands of hectares of mangrove have been planted (Lewis 2005, Kodikara et al. 2017). However, planting efforts often fail, as mangroves are regularly planted at sites with unsuitable hydrological conditions: too deep with respect to MSL, too high frequency of tidal flooding and too much wave impact (Lewis III and Marshall 1998). In fact, mangroves favour a surface elevation between mean sea level and mean high tide (Clough 1982) and prefer areas inundated approximately 30% or less of the time by tidal waters (Lewis 2005). Mangroves can repel anoxic conditions to a certain extent using pneumatophores: aerial roots for gas exchange. Yet, too high inundation frequencies induce mangrove mortality because pneumatophores cannot capture sufficient oxygen (Adams and Human 2016) and salinity in the soil rises to lethal levels (Hossain and Nuruddin 2016). At more favourable sites, inundation free time windows occur that are long enough for recruitment before seedlings are being dislodged by hydrodynamics and/or erosion (Balke et al. 2011b). Therefore, understanding topography of a reference forest is key to find suitable places for restoration. In addition, species that colonize at newly formed deposited sediment along the coastline, are generally more resilient against stresses. For example, *Avicennia ssp.* is more resilient against highly energetic conditions than *Rhizophora ssp.* (Thampanya et al. 2002), and is more resistant to fluctuations in salinity (Hossain and Nuruddin 2016). In many cases, shortcomings of restoration efforts can be attributed to their failure to address root causes of mangrove decline, such as land-use change and unsuitable physical conditions for mangrove survival.

Successful restoration efforts address the root cause of mangrove deterioration and start with a proper baseline survey that outlines present physical conditions (McDonald et al. 2016). Also, a control or reference area where healthy mangroves are present will serve to set proper restoration targets. Choosing for passive restoration that focusses on enhancing natural recruitment by restoring appropriate environmental conditions, is in line with Standards for Ecological Restoration. This is classified as assisted regeneration for intermediate degraded eco-systems (Nathan and Scobell 2012). Passive restoration focuses more on restoration of the abiotic conditions in which mangroves thrive (i.e. the reference system). For example, digging creeks helps restore the hydraulic connectivity which in turn allows for the rapid recruitment of mangroves (Lewis 2001).

Not only from the seaward side, also creeks coming from the landward side enhance flushing and regulate salinity (Lewis III et al. 2016). Blocked channels by for example road constructions may lead to mortality prompted by peaking salinity levels. Early detection of this problem is key to restore the ecosystem, since completely degraded systems are difficult to restore (Nathan and Scobell 2012, Lewis III et al. 2016). However, if a stable or accreting state is acquired and hydraulic conditions are comparable to those of a sheltered area, mangroves are likely to return without active planting (Kamali and Hashim 2011). Apart from hydraulic conditions, flourishing of mangroves also relies on soil properties such as soil pH, bulk density, CEC, nutrients, carbon and organic content (Hossain and Nuruddin 2016). For example, bulk density has a positive effect on root length (Ola et al. 2018), while there is a positive relationship between root length and critical erosion/dislodgement force (Balke et al. 2011c).

Permeable structures (Figure 1.1) are a recognized method that promotes the seaward expansion of vegetation along coastlines (Van Cuong et al. 2015a). The rationale behind the brushwood permeable structures is that by attenuating erosive waves, they trap sediments and as a result elevate the sediment bed level (SBL) at the landward direction of the fences (Dijkema et al. 2010). Often, a network of ditches is created to improve drainage and facilitate colonization of saltmarsh plants. These pioneering plants accelerate the sedimentation process and the increasing bed level makes conditions suitable for other species to come in. The idea was that a similar process could be facilitated using permeable structures along muddy mangrove coasts. Permeable structures would create still water conditions for precipitated sediment to remain stable. Increased bed level and reduced wave impact would generate suitable conditions for mangrove settlement. In turn, mangrove presence would help stabilization and drainage of the soil and reduce the impact of waves and currents. These calm conditions would allow for development of various mangrove species, restore lost mangrove forests and possibly even revert the state of the coast from eroding to accreting (Tonneijck et al. 2015).

In contrast to hard structures such as dykes or seawalls, permeable structures simultaneously allow for the dissipation of wave energy, sediment laden water to pass through and prevent the occurrence of wave reflection and scouring around the structure (Winterwerp et al. 2014). Often hard structures worsen the problem by aggravating erosion due to unanticipated interference with sediment flows and soil conditions (Winterwerp, Borst, & de Vries, 2005). Additionally, brushwood structures can easily be adjusted if needed, while the redesign of hard structures is commonly costly and time consuming (Vuik et al. 2019). Successes of this method has been reported along the coast of the Kien Giang Province of Vietnam in which multiple permeable structure designs have been applied. Within three years half a meter of sediment was deposited behind the fences and mangrove recruitment was enhanced (Van Cuong et al. 2015b). Also in fresh water lakes, brushwood structures were being implemented, which successfully dissipated waves energy to protect reed communities (Ostendorp et al. 1995).

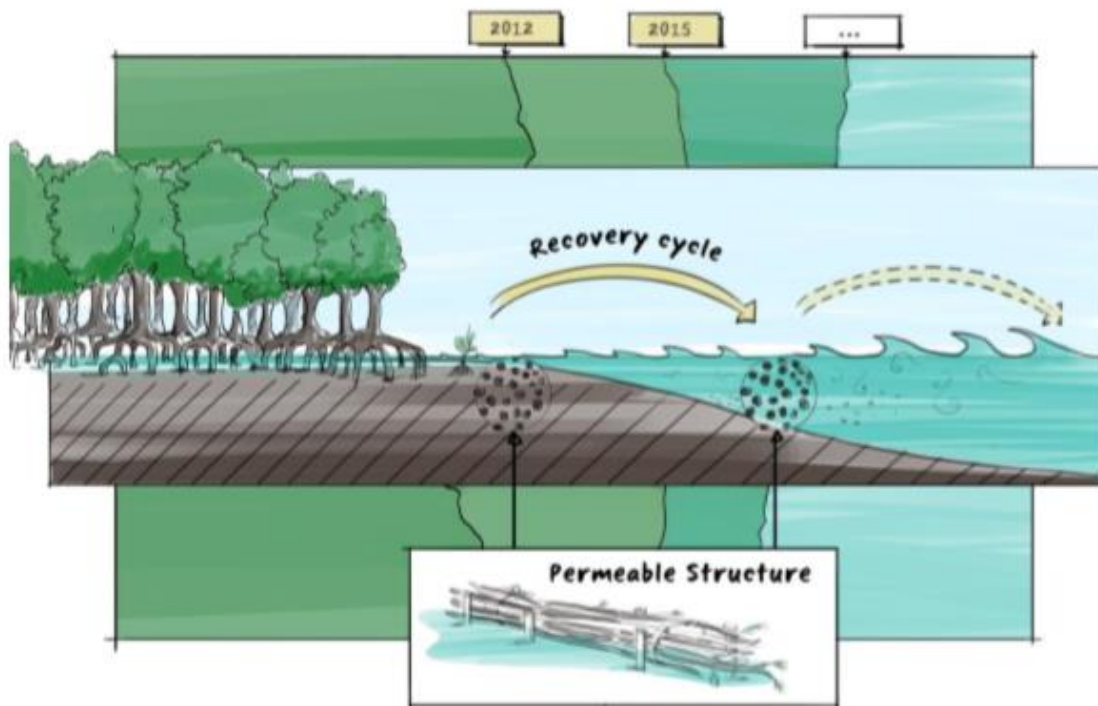


Figure 1.1: Schematics of the physiology of permeable structure. The structure slows currents and dissipates wave energy into the landward direction to mediate sedimentation behind structure. This will foster elevated platforms which are opportune for mangrove recruitment (Winterwerp et al., 2014).

Correspondingly, mangroves were replaced for aquaculture ponds following a general trend of mangrove decline in South East Asia. As a result, the coastline is virtually devoid of mangrove and has shifted towards a state that is constantly eroding instead of slowly accreting. Subsidence further hampers mangrove rehabilitation via two pathways. First, there is less habitat suitable for mangrove settlement. And second, incoming wave height increases which puts more mechanical stress on the sediments and mangroves (Winterwerp et al., 2014). Along the coast of Demak, permeable structures are erected, aiming to alleviate these pressures that force mangrove decline.

In this monitoring report, we elaborate on the effectiveness of permeable structures for mangrove restoration in Demak (Central Java, Indonesia). Our approach concerns testing the method in Indonesia along the heavily inhabited, utilized and eroding coastline of Demak. This area is dominated by small coastal villages and aquaculture ponds that are declining in productivity. We combine coastal restoration with aquaculture rehabilitation and empowerment of local community. Monitoring is performed by small scale monitoring (single structure) and monitoring of the upscaled research location (20km of the Demak coast). In order to test the effectiveness of the permeable structures in restoring the coast the following questions are investigated:

1. Are permeable structures effective in trapping sediment?
2. Can mangrove colonization take place behind the permeable structures?
3. Do mangroves colonize and develop into healthy mangrove forest behind the structures?

To answer these questions spatial and temporal variation in mangrove settlement and changes in sediment bed level were measured. For bed level changes, a simple method for monthly monitoring was developed, using monitoring poles to capture changes in sediment bed level height behind and in front of permeable structures. Also, mangrove recruitment behind the structures was measured. To obtain a good insight in compaction bulk density was measured in cores collected from the field. Here, methods and results are presented and implications of this are discussed to clarify the functioning of permeable structures for mangrove restoration.

2 Materials and Methods

2.1 Site description

The permeable structures are implemented in Demak province along the North coast of Java, Indonesia (Figure 2.1 and Appendix: Locations of PVC measuring poles and permeable structures.). This area is characterized by a tropical climate, dominated by two monsoon seasons. The South Easter monsoon, lasting from May till September and the North Wester monsoon from October till April (Wyrki 1961). Orientation of large-scale residual currents shift with the monsoon seasons. During non-storm events offshore maximum significant wave height is measured to be 1.5 m with a period of 5.5 s. The last 15 years show an average wave height of 0.46 m (Tonneijck et al. 2015). Over the last centuries alluvial sediments have been deposited along the entire coastline (Abidin et al. 2013). During recent decades aquaculture has increased substantially in Indonesia (Paryanti 2006), and has resulted in the loss of large areas of mangrove forest (Richards and Friess 2015, Friess et al. 2019).

From Semarang to the Wulan river delta, the coast shows varying rates of coastline change. Just south of the Wulan river the coast has been stable since 2003 (Wesenbeeck et al. 2015). Further south, where monitoring of the permeable structures takes place, the coast is less stable. Despite progradation taking place very locally behind sandy sea ridges (also known as cheniers), the overall trend is erosive (Wesenbeeck et al. 2015). Approaching the North of Semarang, the erosion gradually increases and is the most severe near the city, which is likely caused by the high rates of subsidence (Chaussard et al. 2013a).

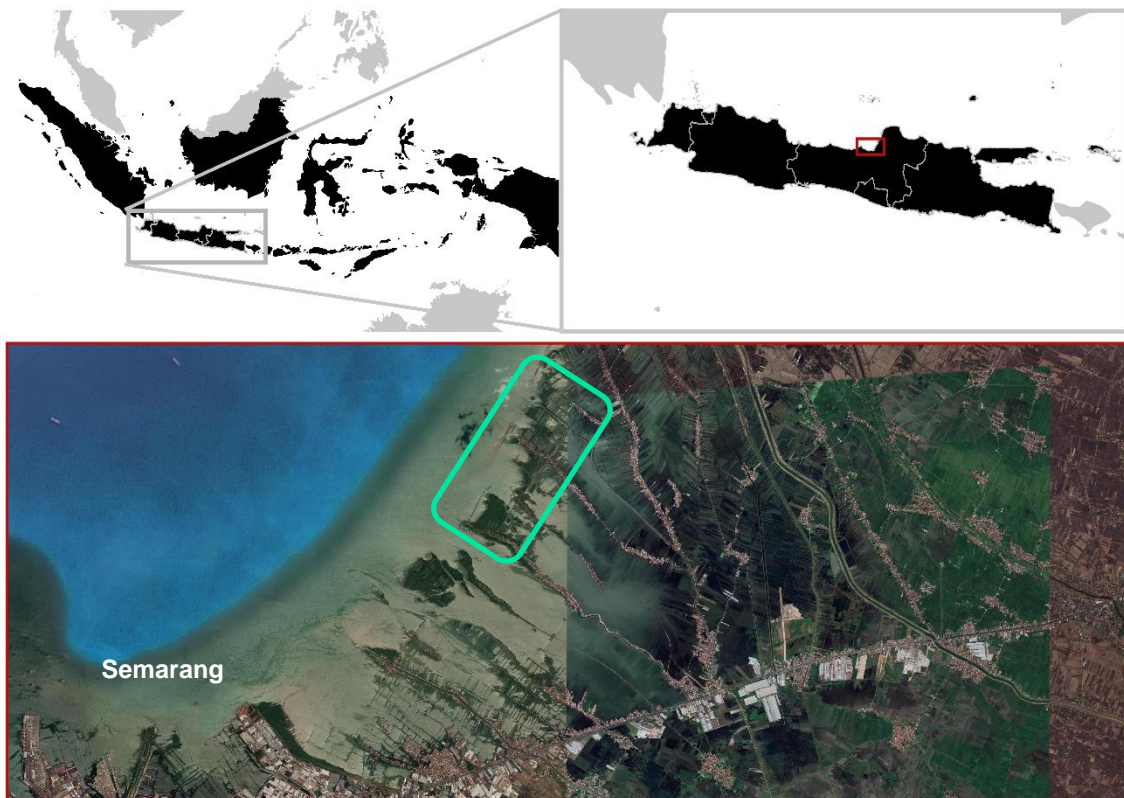


Figure 2.1. Location of the research area is shown by the green rectangular box.

2.2 Permeable Structures

2.2.1 Functional design

Permeable structures are designed to dampen waves and induce still water conditions for sediment precipitation. The permeable structures dampen waves, and limit reflection. Design and material used for the permeable structures went through a series of iterations. Each structure is approximately 100 meters long. Most structures have an opening of about 5 – 10 m in the middle. Initial designs used local materials such as wood, bamboo, twigs or other brushwood. Most recent designs however use PVC measuring poles and are strengthened with concrete. Using the PVC measuring poles required the least amount of maintenance on an annual basis.

2.2.2 Spatial Design

Permeable structures are constructed near the coastline (Figure 2.2), and gradually advance in seaward direction. Once the erosion process has been stopped and the shoreline has accreted to sufficient elevation, mangroves are expected to colonize naturally. The minimal elevation required for successful settlement is expected to be higher than the Mean Tidal Level (MHW) (Balke et al. 2011a). Once mangroves start to increase in size, they contribute to wave attenuation, capture sediment and can (partly) take over the role of the structures.

2.2.3 Maintenance

Coastal communities in Demak are involved in the construction and maintenance of the permeable structures. Over the course of 4 years and along a 10 km stretch of coast in total 48 structures were constructed. Of the 48 structures, 19 were inspected for signs of degradation. This was done by visually inspecting if there were any signs of damage to the pillars, if the pillars were slanted and if the brushwood in the structures was still present. Pristine structures were given a score of 5, while completely degraded structures were given a score of 1.

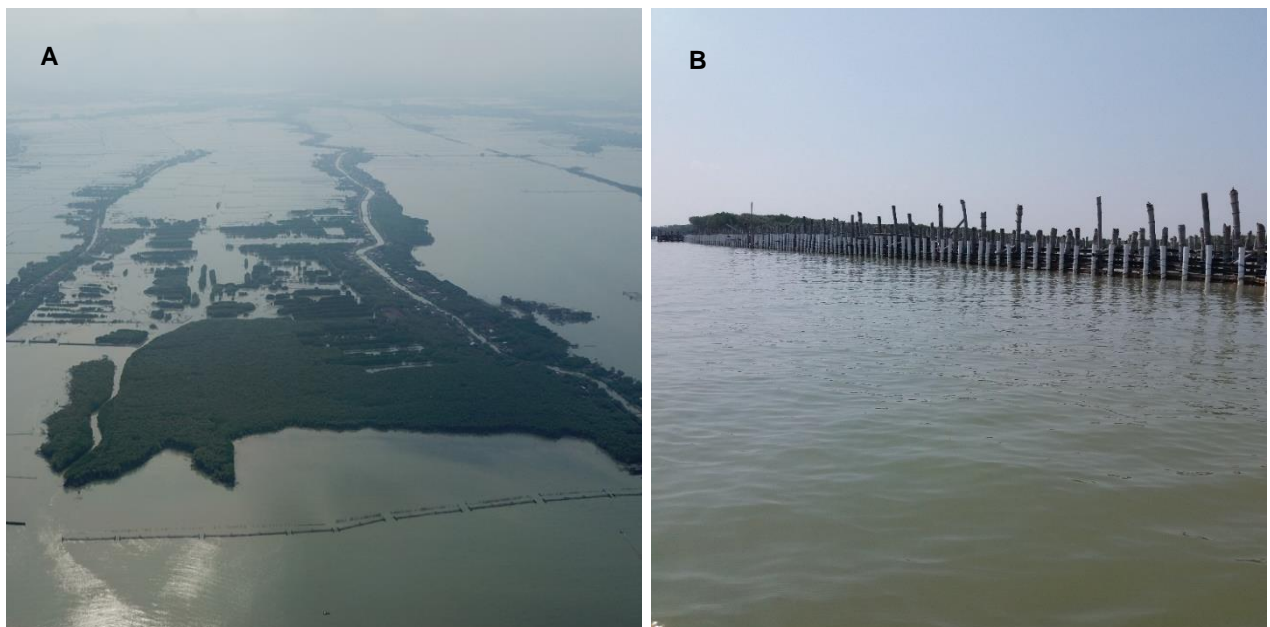


Figure 2.2. Two pictures of the permeable structures. A: Aerial picture taken by drone. The picture is orientated landwards and shows the remaining mangrove patches spread throughout the coastline and creeks meandering. The permeable structures are located seaward from the mangroves. B: Up close picture taken of a structure that is in a pristine state. The large vertical and horizontal beams are in place, and the brushwood filling is still present.

2.3 Sediment bed level time series

2.3.1 Data collection and field design for sediment bed level time series

The aim of the monitoring campaign was to investigate the effects the permeable structures have on sediment bed level (SBL) height. Monthly changes in SBL were measured using vertical measuring poles made from PVC measuring poles, hereby it is possible to capture the net effect of the following processes:

$$\text{Equation 2-1: } SBL(t) = SBL(t_0) + \int_{t_0}^t (D - E - C) dt$$

Where D, E and C respectively stand for: deposition, erosion and consolidation.

Although an easy and effective way to measure net elevation of the sediment bed, it remains unknown what the relative contribution is of each of the three parameters. Each measuring pole has a length of 2 meters, an inner diameter of 15 cm and was placed 1 m in the sediment bed (Figure 2.3). Thus, at the onset of the monitoring (T_0) the SBL is exactly at the middle of the measuring pole. At each subsequent time step of one month, the SBL was measured. This was done by taking a measuring stick and gently placing the next to the measuring pole. The SBL was measured multiple times, each time the stick was placed slightly further from the pole, to maximum of 15 – 20 cm. The average is eventually noted.

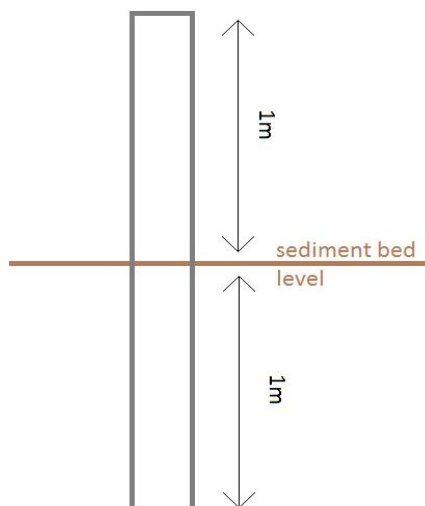


Figure 2.3. Schematic representation of measuring pole placement at time of placement (T_0).

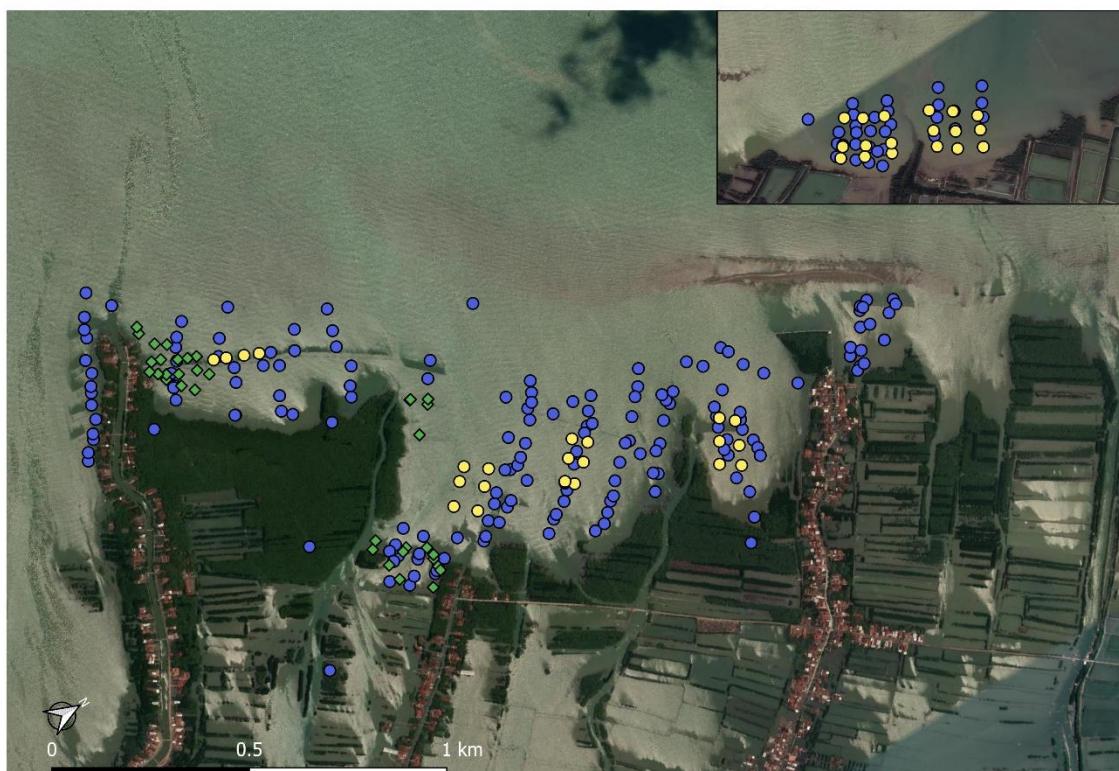


Figure 2.4. Satellite image of study area showing all monitoring locations. The yellow circles represent the monitoring poles that were installed in May 2015 (**Cohort A**), the green diamonds the poles installed in February of 2017 (**Cohort B**). The blue circles are locations of (**extra**) sampling during monitoring campaign in September of 2019.

In total 80 monitoring measuring poles were installed during 2 different field visits (cohort A & B, see Table 2.1). Although the measuring poles were placed in 2015, monitoring of the poles for the time series did not start until 2017. This was because of difficulties with monitoring that arose at the onset of the project.

The measuring poles were placed and monitored at the seaward and landward side of permeable structures and at locations where no structures were present. Seaward and remotely located measuring poles were classified as *controls*. Measuring poles landward from the structures were classified as *grid*.

Measuring poles were installed at locations where the permeable structures were already present. This allowed for paired comparison between measuring poles within structure, i.e. comparing measuring poles at the seaward side of a structure to measuring poles at the landward side of the same structure (*controls* vs *grids*). Some permeable structures were constructed after the instalment of the measuring poles. This gave the opportunity for a time series analysis of SBL, i.e. comparing SBL at a single measuring pole but at different moments in time (i.e. before and after treatment).

2.3.2 Statistical analysis of in sediment bed level height

Some measuring poles were lost due to storm events. These poles were removed from the data set. Because the instalment date for each cohort differs and sediment bed level relative to the pole at the moment of placement was measured, cohort *B* was excluded from the analysis. Cohort *A* has the longest ongoing monitoring data set and was therefore used for long-term trend analysis of SBL. Because SBL height affects inundation frequency, and thus deposition rates, comparing and/or aggregating data from different cohorts would result in comparing data at different time steps (e.g. for cohort *A* at T_n and for cohort *B* at T_0). Hence, only data from cohort *A* was used for this analysis.

To test the hypothesis that permeable structures have an effect on SBL a statistical model was used, i.e. a Linear Mixed Model (Bates et al. 2015) In other words, SBL-height of *grid* treatment is compared to SBL-height of *control* treatment. Linear Mixed Models (LMM) are especially useful for repeated measurement data, when dealing with non-independent observations. A mixed model allows for specification of a deterministic and random term. Classification of the measuring pole (i.e. *grid* vs *control*) was used as the fixed component (i.e. deterministic) of the LMM. The random component was systematically varied in order to test which combination of explanatory variables described the dependent variable (SBL) the best. An ANOVA is used to compare AIC (Akaike information criterion) values between the different models.

2.3.3 Statistical analysis of sediment bed level before and after treatment.

Only the data points from the PVC measuring poles that were placed prior to the instalment of a permeable structure were used. These poles were from cohort *B*, and consisted a total of 24 locations, 12 of which were grid poles. As the same measuring pole was compared before and after treatment, a standard paired t-test was used for comparison of data values. Data points of the PVC data points 1 month before the treatment were averaged. These were then compared to the mean of the data points 1,2 and 3 months after treatment for the same PVC measuring poles. This was done for the PVC measuring poles that after treatment became *grid* and for the PVC measuring poles that stayed *controls* after treatment. Because construction of the permeable structures also disturbs its local surroundings, a comparison is done for the first three months. Hereby any disturbances to the SBL caused by the construction are expected to have levelled out with its surroundings.

2.4 Spatial mapping of sediment bed level in relation to mean sea level

2.4.1 Data collection and field design for spatial mapping of sediment bed level

Additional SBL measurements were taken in order to create a spatial map of sediment bed level. High spatial density of sampling helps with the production of an interpolated spatial map. The aim is to link spatial variation in SBL to structure placement and *in situ* variation in habitat (i.e. chenier presence). Using a marked stick with a circular disk attached to the bottom, the SBL was measured at location where there are no PVC measuring poles.

In order to compare measurements of the measuring poles, they needed to be calibrated to mean sea level (MSL). The time and location were documented using a GPS. This information is used as input for calculating SBL relative to MSL using a tidal model based on Semarang tidal gauge measurements. SBL was measured at a total of 280 locations throughout the study site (Figure 2.4). The additional sample locations for measuring SBL were taken as transects perpendicular to the permeable structures. Half of a transect was on the landward side of a structure, the other half on the seaward side.

2.5 Spatial mapping of Soft mud layer

2.5.1 Data collection and field design for spatial mapping of soft mud layer

Soft mud layer (SML) can play an important role in the settlement success of mangrove seedlings (Balke et al. 2013). By creating a spatial map of the SML, it is possible to link spatial variation of SML to hybrid structure placement. SML was measured, using half a sphere of known weight and volume. The weight was calibrated for the half sphere to penetrate mud up to 1.35 kg/dm³, which is very close to the interface between fluid mud and consolidated material (Mehta 1986). The tool has a weight of 19.0kg and a diameter of 12.5cm (Figure 2.5). A marked rod is gently placed on the surface of the bed level to measure the depth below the water surface. At each location, this was repeated multiple times in order to more accurately derive the depth of the bed level. After this, the weight volume is deployed from a stable position and gradually sunk until it can no longer penetrate the sediment interface. Next, the distance from the water surface until the top of the sphere was measured. In November of 2019, at 203 locations SML was measured. Site selection for SML measurements was based on expected variability, i.e. larger variability perpendicular to the coast compared to the parallel plane. Samples were taken in transects perpendicular to permeable structures with a spacing of 50m. Natural variation that occurs in the system was also taken into account. Samples were taken near cheniers, open ocean and near mangroves. The other sampling locations were near the structures.

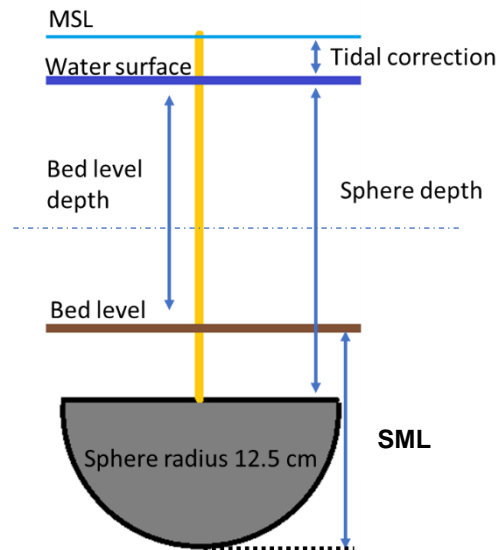


Figure 2.5. Schematization of soft mud layer measurement method using a half sphere.

2.5.2 Calculation of soft mud layer

The SML was calculated by adding 12.5cm (sphere radius) to the measured sphere depth (Figure 2.5). Next the depth of the fluid mud was determined by subtracting the end depth by the measured SBL at the same location.

2.6 Bulk density measurements

2.6.1 Data collection and field design for consolidation

Consolidated fine sediment habitat helps increase changes of successful establishment of mangrove seedlings (Balke et al. 2013). The measurements are thus dedicated to understanding the dynamics between permeable structures and the consolidation of fine sediments. At all pole locations the top layer of undisturbed sediment was sampled separately and stored in a 50ml beaker. The cores were sampled using a PVC pipe of 3 cm diameter and 150cm length. The sampler was pushed in as deep as possible. The pipe was never pushed to its maximum depth of 150cm. Upon extraction of the core from the soil the max core length was established. This was done by measuring the distance of the top of the pipe to where the sediment reached inside the pipe. While maintaining the structural integrity of the core, it was pushed out. Depending on the total length of the core, sub-samples were taken at a minimum of 10cm intervals. Each sub-sample was bagged and tagged. Exposed positions were seen as *controls*, on the seaward side of permeable structures. In order to obtain information about the consolidation status sediment cores were sampled. This was a combination of taking 10 core samples at previous sites and 45 cores and new sites.

2.6.2 Bulk density calculation

Using the sediment from the sub-samples, bulk density was measured within 24 hours of sampling. This was done *in situ* in order to avoid any physical and chemical alterations to the sample. Wet bulk density was calculated using the following equation:

$$\text{Equation 2-2: } \text{Wet bulk density} \left(\frac{g}{dm^3} \right) = \frac{\text{wet mass (g)}}{\text{volume (dm}^3\text{)}}$$

The *wet mass* of the samples was calculated by:

$$\text{Equation 2-3: } \text{Wet mass (g)} = \text{mass of full flask (g)} - \text{mass empty flask (g)}$$

And the *volume* of the sample was calculated by adding water to the flask containing the sample. *In situ* water was known density. The water was added until the flasks was full. The added water was weighed before, giving rise the final equation:

$$\text{Equation 2-4: } \text{Volume (dm}^3\text{)} = \text{Pycnometer volume (dm}^3\text{)} - \frac{\text{water weight (g)}}{\text{water density} \left(\frac{g}{dm^3} \right)}$$

2.7 Mangrove count data

2.7.1 Data collection and field design for mangrove count

The aim of mangrove monitoring is to test if the permeable structures contribute to the successful establishment of mangrove seedling settlement. All visible mangroves were counted, from seedlings and saplings to large mangrove trees. There was no distinction between mangrove species, however at some location's mangrove planting took place. These trees were not considered. Mangroves were counted on a monthly basis, keeping track of any temporal variation in mangrove count that could be related to climatological variables. Mangrove height was noted in size classes: 0-10cm, 10-20cm, 20-30cm, 30-50cm, 50-100cm, 100+ cm. Settlement was also related to measured sediment characteristics, i.e. SBL, SML and bulk density. Mangrove count was monitored at 14 of the permeable structures.

2.7.2 Temporal and spatial correlation of mangrove data

For each of the permeable structures where mangrove data was collected temporal plots were made. Data of SBL (2.4) and SML (2.5) collected for spatial mapping and data for bulk density (2.6) were related to mangrove count.

2.8 Software

All data was analysed and processed using python (v3.7) and R (3.5.3) in RStudio (1.1.456) . For python a differs set of packages were used: *statsmodel* (v0.10.1), *scipy* (v1.2.1), and *linearmodels* (v4.13). With R the packages *lme4* (1.1-21) was used.

3 Results

3.1 State of permeable structures

Table 3.1. Pairwise comparisons between the different states of the structures. State could vary between 1-5 (1 = degraded, 5 = pristine). The hypothesis states that means of SBL are equal between groups and can be rejected with $p < 0.01$. Kruskal–Wallis test indicated statistical difference between groups ($p < 0.000$). Table below shows the Post hoc test results of conover's test using "holm" method for p -value adjustment. Significant values are shown in bold.

Qualitative State	0	1	2	3	4	5
0	-	1	0.000	0.000	0.000	0.000
1	1	-	0.000	0.000	0.000	0.000
2	0.000	0.000	-	1	0.883	0.131
3	0.000	0.000	1	-	1	0.835
4	0.000	0.000	0.883	1	-	1
5	0.000	0.000	0.131	0.835	1	-

For nineteen permeable structures, the physical state was monitored from 2017 till 2020 in a qualitative manner using a scale from 1-5 (Table 3.1 & Figure 3.1, and see appendix C for examples of different qualitative states). The data used for this analysis, is derived from monitoring of the PVC measuring poles for all years. Non-parametric statistical analysis indicated that the state of a structure had a significant effect on the mean SBL (Kruskal–Wallis test, $p < 0.000$). Post-hoc pairwise comparison using conover's non-parametric test showed that when a structure had a qualitative state of 1, bed level changes were comparable to bed level changes in control plots (Control measurements are indicated as 0 in Figure 3.1). Structures with states between 2 – 5 didn't show a significant inter specific difference in mean SBL. This means that even though the status was classified into 5 categories, differences were only detected between category 1 and all other categories.

As stated above, the qualitative state of each structure was monitored. How the state evolved over time for each structure can be seen in Figure 3.2. Yearly maintenance of structures is a necessity, however not every structure was properly maintained (e.g. kkp3, kkp7, kkp8, pu03). Structures such as tw2.1 and su2.2. show a sharp increase in SBL when quality of structure reverts from bad to good. When the state of a structure changes, the trend of SBL also changes, albeit with some lag. For example, when a structure is in such disarray that it is deemed to have "bad condition" an upward or stable trend in SBL, usually turns into a downward trend (see structure 11. And 11.2 in Figure 3.2). The opposite also holds.

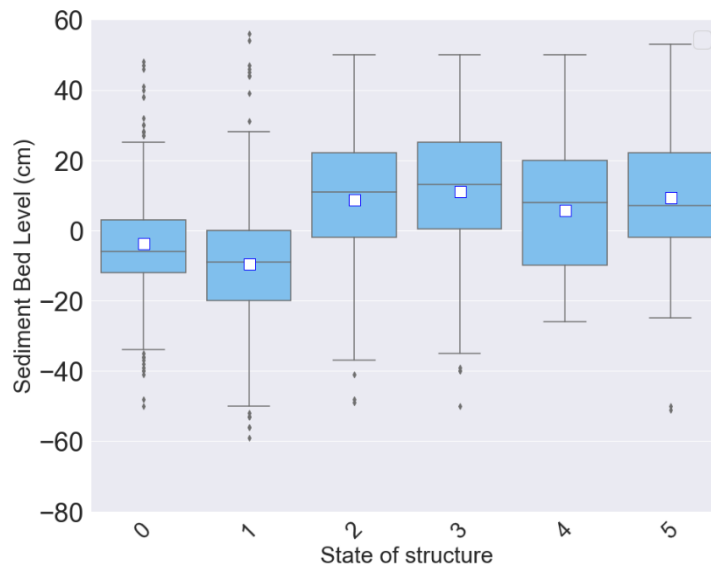


Figure 3.1. Sediment bed level measurements arranged by qualitative state of a permeable structure. State of 0 indicates the control measurements. The white squares indicate the mean). The data used for this analysis, is derived from monitoring of the PVC measuring poles for all years (i.e. cohort A & B).

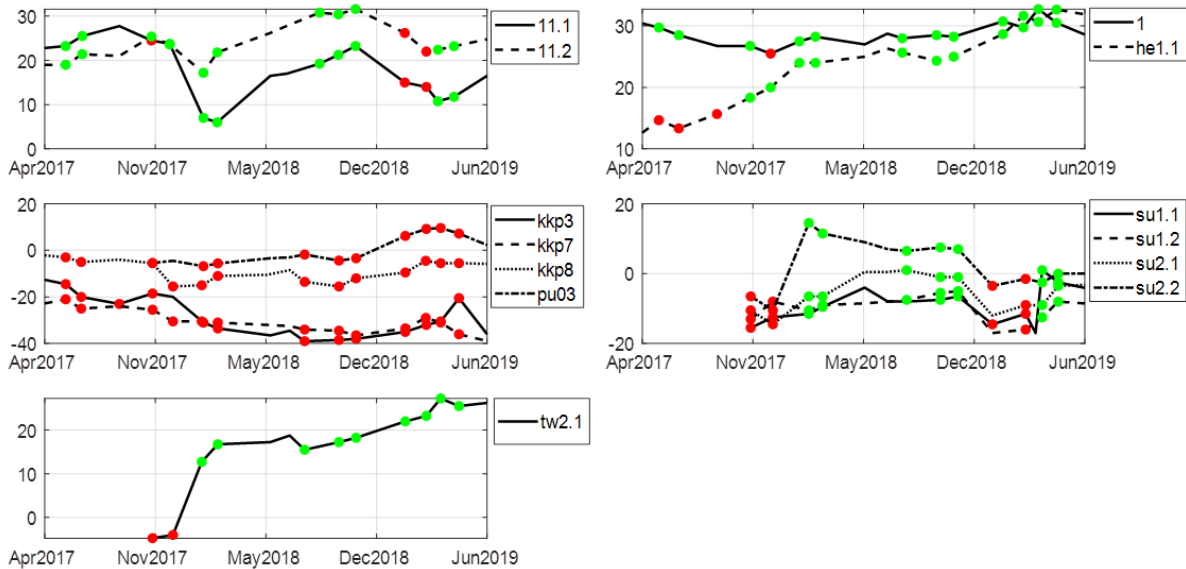


Figure 3.2. The above graphs show the change of sediment bed level height (cm) on y-axis and time on the x-axis. Note the different y-scales per graph. Each line represents the average sbl of the grid measuring poles of each structure. The green and red dots represent the state of the structure. The green dots a state of 2-5 and a red dot a state of 1 (see Figure 3.1). The graphs cluster the structures that are within proximity of each other. The data used for this graph, is derived only from the PVC measuring poles near their specific structures.

3.2 Sediment bed level results

3.2.1 Time series

For the assessment of the time series, data was used from cohort A. Data used for the assessment was gathered in the period of 2017 – 2020. A total of 1241 measurements were taken during this period (Table 3.2). From 2017 and onward, monthly SBL mean of grid measuring poles was higher compared to the mean of control measuring poles (Figure 3.3). Although there was no monitoring in the initial months after measuring pole placement, it is expected that the deviation between control and grid took place in the first few months. This can be seen in the graphs that compares SBL before and after the construction of permeable structure (Figure 3.6). The difference between grid and control measuring poles remained constant over the monitoring period, varying between 20 – 30 cm. Measurements from the control poles showed larger variation.

Table 3.2. Descriptive statistics of Sediment Bed Level categorized by year, location and overall. As described in section 1.1, the data points grid measuring poles where the state of the structure was 1, have been removed. **Type:** Either control (c) or grid (g). **N:** Sample size, **SD:** Standard deviation. The minimum and maximum values for each sub category are also shown. Finally, the corresponding cohort is also shown.

	Total N	Type	N	Mean (cm)	SD (cm)	Minimum (cm)	Maximum (cm)	Cohort
All	1241	c	858	-4.6	14.1	-51	-13	All
		g	383	17.3	17.5	-27	6	
Year								
2017	352	c	305	-7.7	12.1	-50	40	All
		g	47	23.7	12.7	-10	50	
2018	320	c	222	-5.4	13.1	-37	35	All
		g	98	14.1	14.3	-19	50	
2019	425	c	254	-1.9	15	-51	38	All
		g	171	16.7	17.5	-25	53	
2020	144	c	77	1	17.1	-45	45	All
		g	67	19.2	23	-27	58	
Location								
Bedono	349	c	220	-4.9	15.9	-38	45	A
		g	129	23.4	11.1	-4	52	
Bogorame	518	c	359	-5.5	15.1	-51	40	A
		g	159	26.2	12	-10	58	
Surodadi	192	c	279	-3.2	10.6	-31	24	B
		g	95	-6	10.2	-27	21	

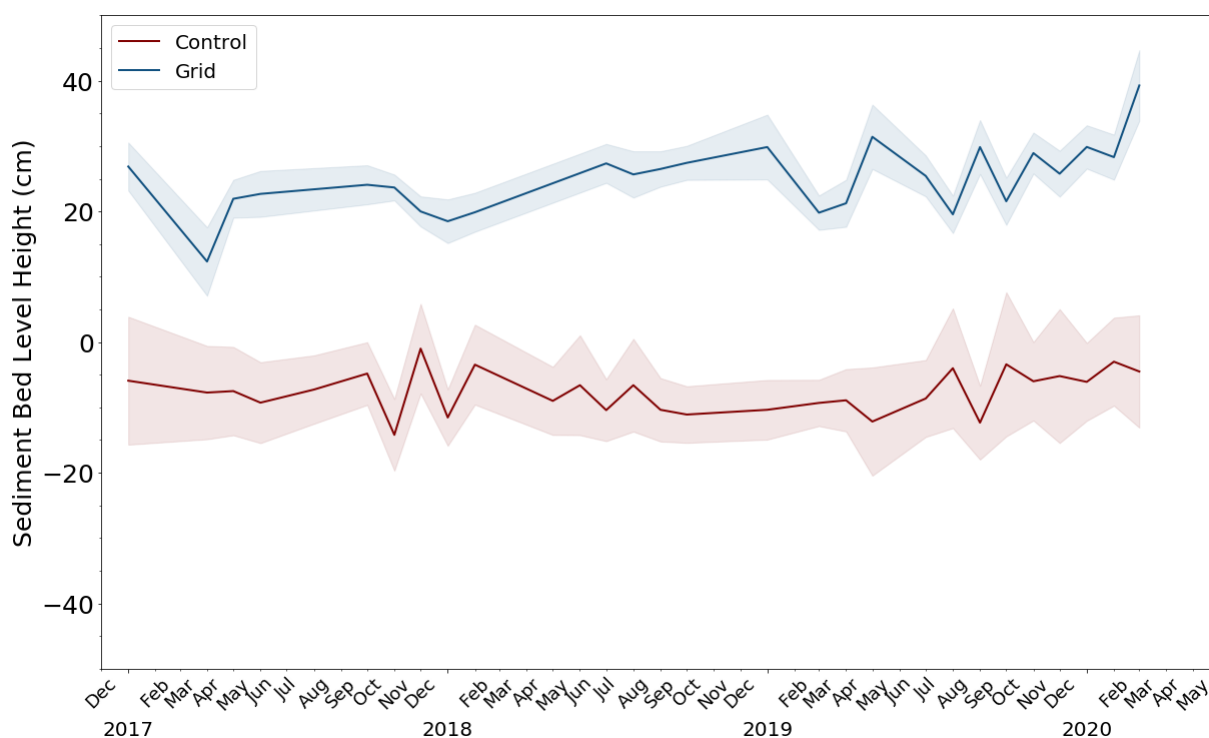


Figure 3.3. Monthly average (solid line) and standard error (shaded area) for measurements of SBL at control (red) and grid (blue) locations. Monitoring started after the initial placements of the PVC measuring poles (in 2015), hence the plotted lines do not start at the initial conditions of 0 cm of SBL. The data used for this graph, is derived from the monitoring PVC measuring poles of cohort A, i.e. the poles that were placed in 2015.

A series of linear mixed effect models (LMM) were compared as to how well they describe and predict variation in SBL, the dependent variable. Such models have independent variables that are either fixed or random effects. The binary variable: grid/control, was used as the fixed component of the model. For the random component of the model, a series of different variables were used and selected through a stepwise approach. For random components it is also possible to have random intercepts and random slopes, both were varied systematically (Figure 3.4). The random effects assessed were: time, region and structure. Adding month or year did not improve the quality of the model (Table 3.3). The LMM with lowest AIC ($p < 0.001$) has control/grid as fixed effect, and control/grid embedded per structure as random effect, with the model having a random slope and intercept per structure (model 3, Figure 3.4). Meaning that the intercept and linear relationship between SBL and control/grid differed per structure. On average SBL of grid measuring poles was 27 cm higher than control measuring poles, with an average intercept of -21 cm. At best, the random component of the model explained 76% of the variance in SBL. Adding a second fixed effect, in this case the state of the structure (model 6), did not lower the AIC below 6064.

Table 3.3. Table shows the different models tested. In all cases control/grid was fixed component. For the random component the variables month, year, structure and state of structure were used. The percentage of the residual variance is shown, that is, the remaining percentage of variance not explained by the random component. The AIC values are estimators of the quality of the models. The smaller the AIC, the higher the quality.

Number	Model	Slope (Std)	Residual Variance of Random Component	AIC
1	$sbl \sim control_grid + (1 month) *$	20.03 (1.8)	100%	6691
2	$sbl \sim control_grid + (1 structure) *$	27.72 (1.3)	42%	6221
3	$sbl \sim control_grid + (control_grid structure) **$	17.14 (9.1)	24%	6064
4	$sbl \sim control_grid + (1 state\ of\ structure) *$	26 (1.5)	66%	6416
5	$sbl \sim control_grid + state\ of\ structure + (1 structure) *$	27 (1.3) & 0.6 (0.5)	44%	6222
6	$sbl \sim control_grid + state\ of\ structure + (control_grid structure) **$	18 (9) & 0.6 (0.5)	25%	6064

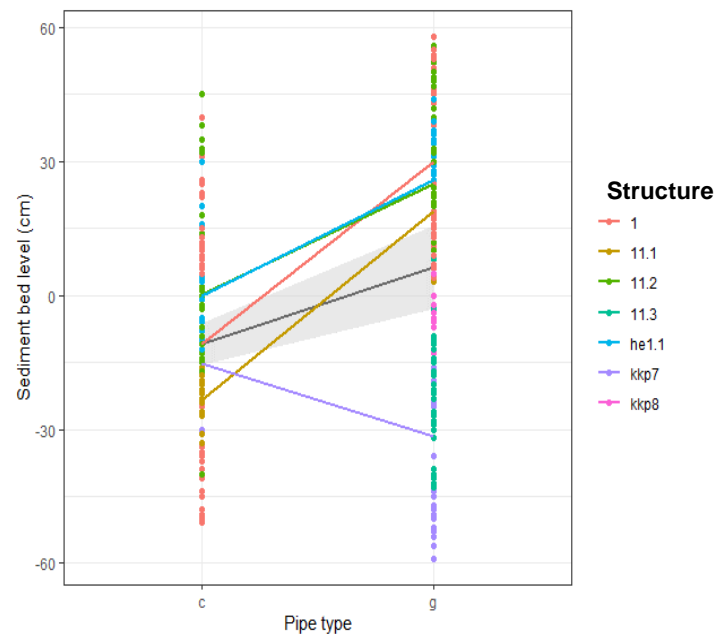


Figure 3.4. The figure depicts the results of a linear mixed effect model. The figure shows the results of the 3rd model as seen in Table 3.3. The coloured lines represent the trends for the different structures. The dark grey line, with light grey band represents the average trend with SD respectively.

3.2.2 Spatial variability of time series

Large variation can be seen between locations (Figure 3.5, A) and between structures (Figure 3.5, B). Thus, where a structure is placed can greatly influence the SBL. This corresponds with the statistical analysis in the previous section. Except at one location, control measurements are on average lower than grid measurements at the village level (Figure 3.5, A: Surodadi 1). At the structure level, control measurements are sometimes higher than grid measurements.

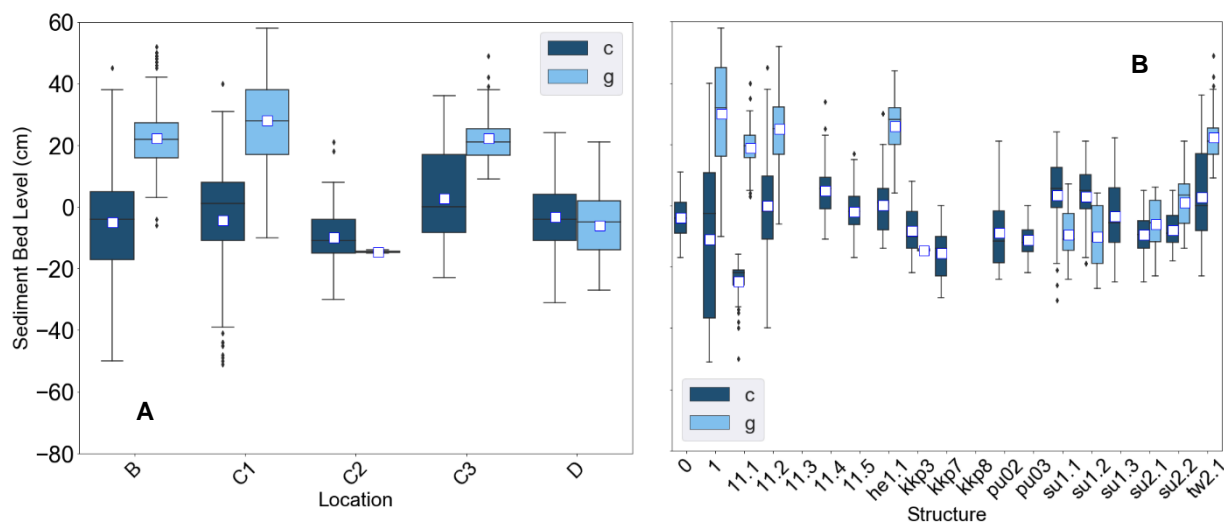


Figure 3.5. Boxplots of Sediment bed level measurements arranged by location (a) and structure (b) for grid measurements (g) and control measurements (c). The white squares indicate the mean. The data used for this graph, is derived from the monitoring PVC measuring poles of all cohorts, i.e. the poles that were placed in 2015 and 2017.

3.2.3 SBL before and after placement of permeable structure

For three structures PVC measuring poles were placed prior to structure instalment (SU, SU2 and TW, see Figure 2.1). This allowed for a paired comparison within location. For the statistical comparison, the before-treatment-sample was averaged for the three months leading up to the construction. The after-treatment-sample was averaged for the first three months after the construction. This was done in order to compensate for any “noise” in SBL caused by construction activities. A Non-parametric Wilcoxon signed rank test shows that for 2 out of the 3 structures there is a significant difference SBL height, before and after placement of the structure (Table 3.4).

Structures SU and SU2 are situated within 100 m from each other (Figure 2.1). Although SBL at SU is always lower than at SU2, they do show similar trends, implying a local effect influencing SBL height. The first three months after placement of structure SU, SBL increased no more than 10 cm (Figure 3.6). Eventually it never reached higher than -10 SBL. The control samples at location SU, are the only measuring points that show an increase after pole placement (Figure 3.6). In fact, throughout the entire monitoring campaign of these control points, the SBL remains higher than their corresponding grid measuring points. Prior to structure placement, the control points of SU2 and TW show a similar trend to their corresponding grid measuring poles. A year after construction event the control points eventually reach similar SBL elevation levels as shown by the grid measuring poles.

Table 3.4. Results of the Wilcoxon signed rank for three structures. The columns n1, n2, m1, m2 respectively represent the number of monitoring points before treatment, number of monitoring points after treatment, median before treatment and median after treatment. p shows significance value. Brackets in columns n1 and n2, indicate the total of pseudo replications. In other words, 4 PVC measuring poles monitored for 3 months, giving a total of 12 data points.

Structure name	n1	n2	m1	m2	p
SU	4(12)	4(12)	-12	-10.5	0.181
SU2	4(12)	4(12)	-8	5	0.008
TW	4(12)	4(12)	-3.5	15.5	0.002

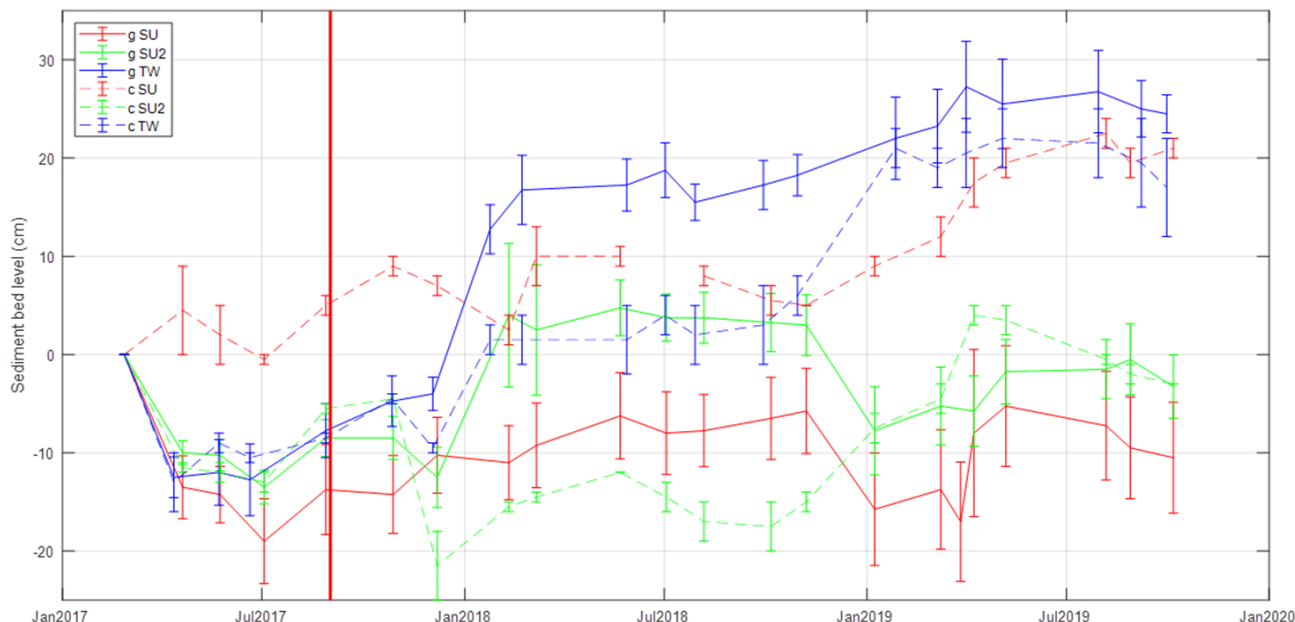


Figure 3.6. The coloured lines with error bars portray average ($\pm 1SE$) sediment bed level behind a permeable structure (SU (red), SU2 (green) and TW (blue)) as a function of time. The vertical red line displays the moment in time the permeable structures were constructed (September of 2017). The dotted lines represent the control measuring points.

3.2.4 Spatial measurements of sediment bed level and Soft mud layer

During the monitoring campaign of 2019, SBL measurements were calibrated to MSL. These show that on average the locations behind structure had an SBL (with respect to MSL) 20 cm higher, compared to locations in front of or in the absence of structures (Figure 3.7). This 20 cm difference corresponds well with what is seen at in the temporal measurements (Figure 3.3). The SBL is highest at sheltered locations, either those sheltered by the permeable structures or by the chenier present in the research area (Figure 3.9).

The thickest layer of fluid mud is found at the locations where the largest deposits of sediment were found and at other sheltered locations. In other words, whenever SBL was high and behind a structure, was the SML. The latter implies that fluid mud is responding differently than SBL to permeable structures. The field observation show that grid locations have a thicker layer of fluid mud, on average about 2 cm Figure 3.8.

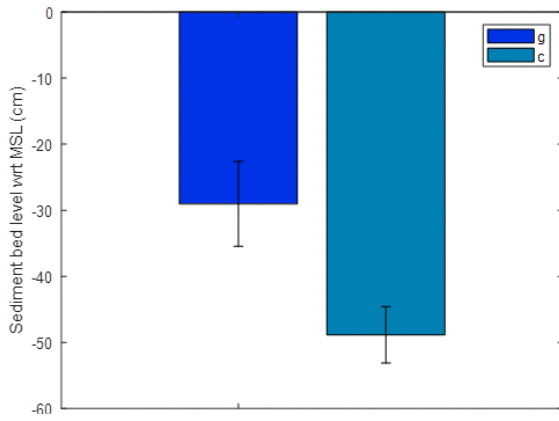


Figure 3.7. Bar chart showing average (+1SE) sediment bed level with respect to MSL for grid (n=89) and control locations (n=61). Measurements were taken in November of 2019.

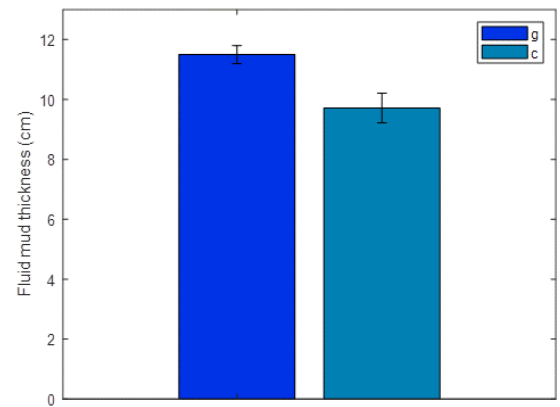


Figure 3.8. Bar chart showing average (+1SE) Soft mud layer for grid (n=89) and control (n=61). Measurements were taken in November of 2019.

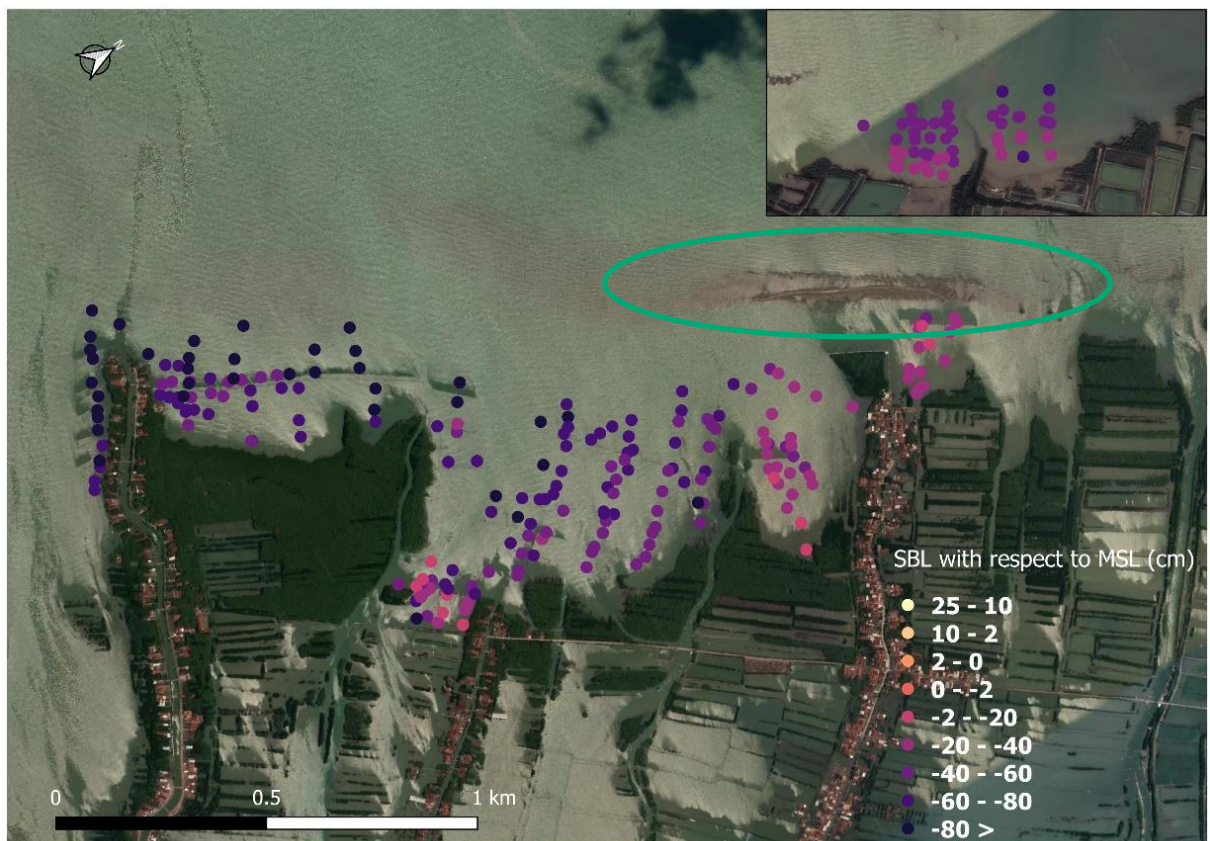


Figure 3.9. Figure depicting the spatial variation SBL with respect to MSL (cm). These measurements were taken in September of 2019. The large green circle shows a chenier in front of some of the monitoring locations. The chenier is likely to have dampening effect on incoming waves.

Distance to structure

The results of the spatial measurements of SBL and SML (Figure 3.7 & Figure 3.8) are also shown in relation to the distance to the nearest structures (Figure 3.10 & Figure 2.1). The bulk of SBL and SML measurements were taken within the first 50 meters of a structure and no clear trend is visible in relation with distance. This shows that for at least the first 150 meters of area on the landward side of the structures there is a homogenous distribution of these two parameters.

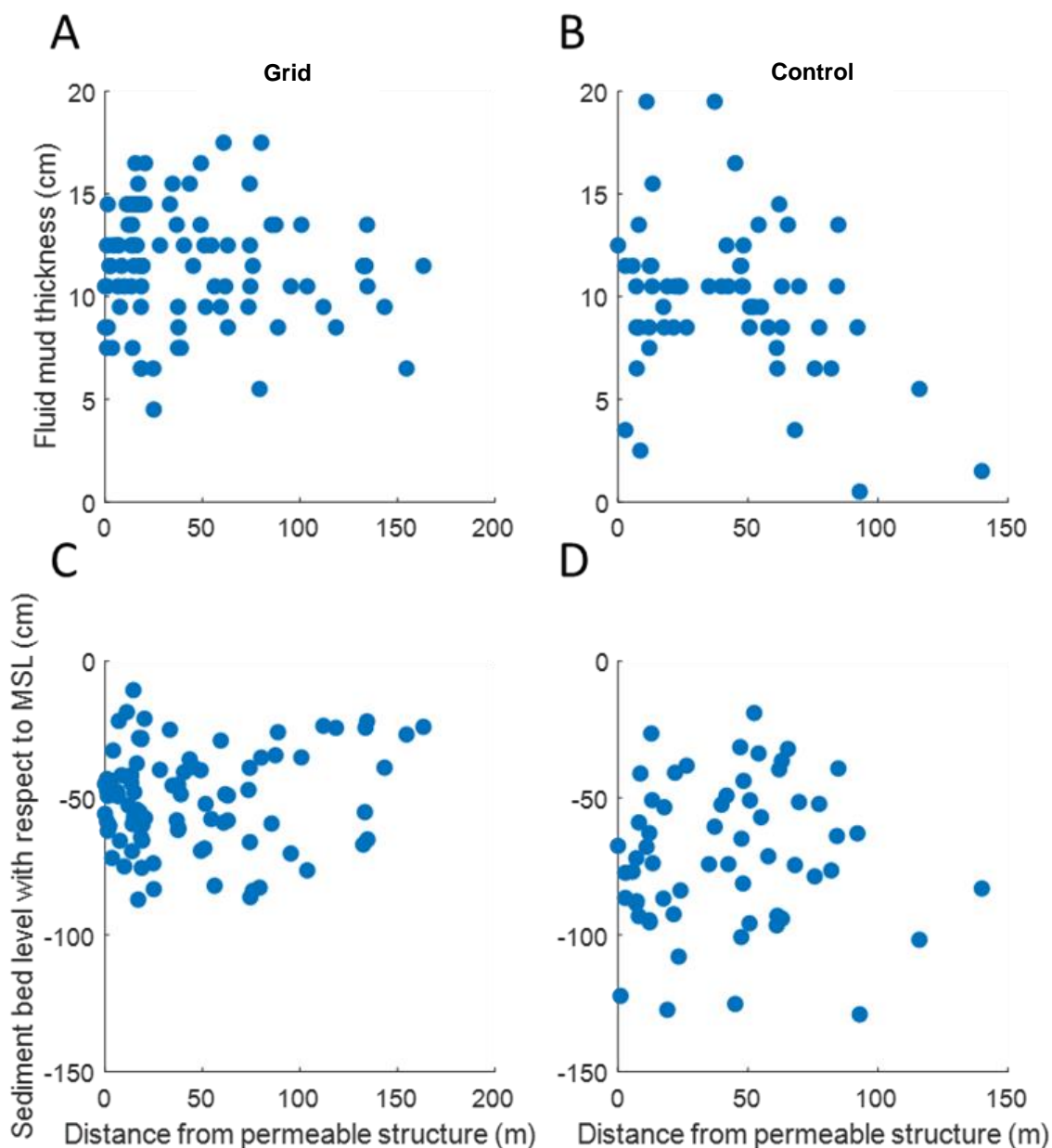


Figure 3.10 **A)** Soft mud layer at locations behind the structures as a function of distance from permeable structure; **B)** Soft mud layer in front of the structures as a function of distance from permeable structure; **C)** SBL at locations behind the structures as a function of distance from permeable structure; **D)** SBL at locations in front of the structures as a function of distance from permeable structure. The data used for graph was taken in 2019 at 150 ($c = 61$ and $g = 89$) locations spread throughout the research area.

3.3

Mean sea level

During the initial spatial design the location of the structures were envisioned to be as near to the coast as possible (Tonneijck et al. 2015). They were constructed within the intertidal area at an elevation near the mean sea level mark. However, a field survey in September of 2019 shows that all structures were placed more than 20 cm below MSL (Figure 3.11). Locations where SBL increased substantially (i.e. HE1, and TW) were also below MSL

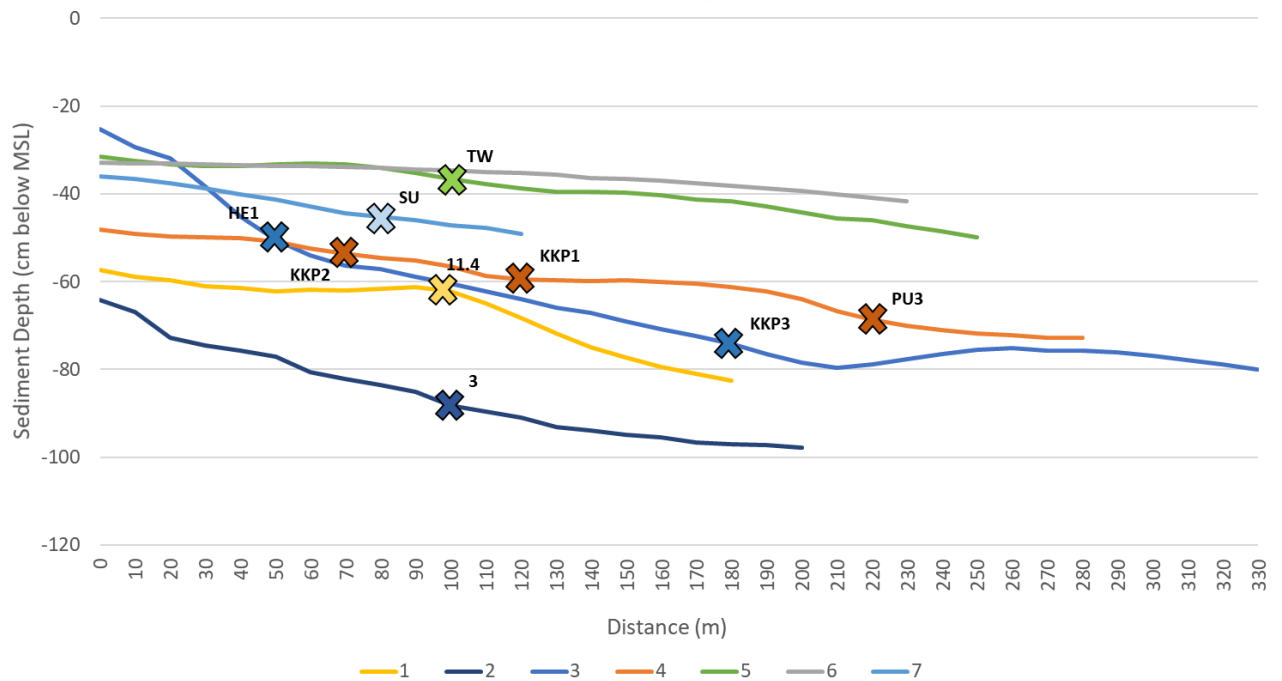
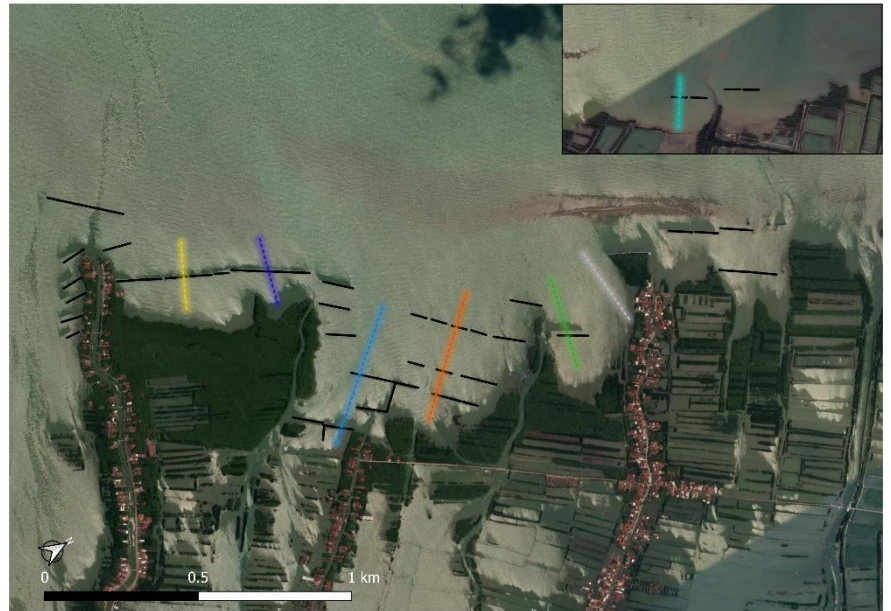


Figure 3.11. The top figure shows a satellite image of the research area. The black lines represent the locations of the permeable structures. The colour dotted lines represent transect lines, the colors correspond with the those in the graph. The transects start near the coast line (distance = 0 (m)) and are drawn seaward. Depth was measured along the transects. The extracted data is plotted in the bottom figure. The graph shows the depth of the SBL (cm) in relation to the MSL. Hence, this is the water depth, or bathymetry. The crosses correspond to the location of the permeable structures along the transect. The monitoring data for these transects was taken in November in 2019.

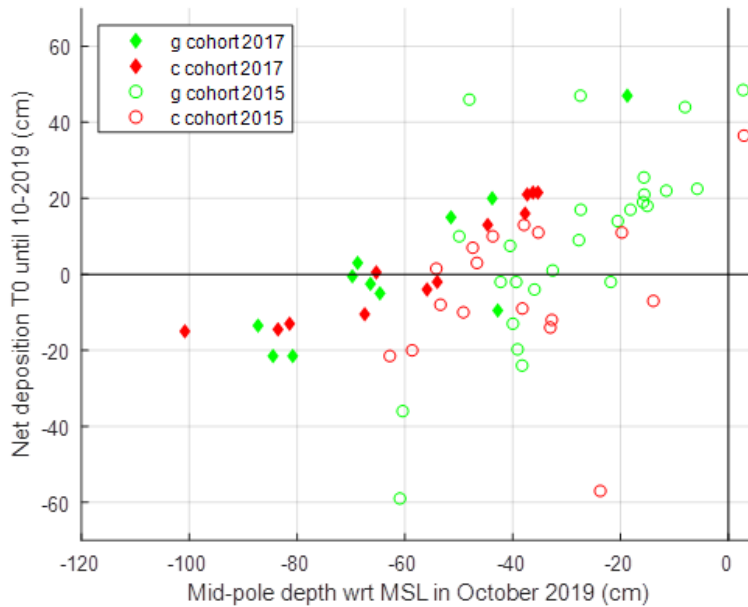


Figure 3.12. The above figure shows the results of measurements that were calibrated to MSL (paragraph 2.4.). The y-axis represents the net deposition since placement of structure. That is, the delta between SBL at moment of construction (either in 2015 or 2017) vs. the most recent measurement (October 2019). The graph shows two different cohorts, 2015 (circles) and 2017 (diamonds). The x-axis represents the depth of the centre of the pole with respect to MSL, at the moment of measuring SBL in October of 2019. The monitoring data used for this graph is derived from the PVC measuring poles associated with three different structures. Red represents measurements at control locations, green represents measurements at grid locations.

Sediment deposition was positively correlated with depth (Figure 3.12). In fact, there is a strong linear trend visible. The higher a pole is situated within the intertidal zone; the more deposition has occurred since initial conditions.

3.4

Mangrove Count

Mangrove settlement was observed at 13 of the 19 structures that were monitored (Figure 3.13). The data shows that mangrove establishment occurs during peak events. Large numbers of mangrove settlement can be seen in the early months of 2017, 2018 and 2019. After a settlement event, numbers steadily increase, as the remaining mangroves increase in height. Only one structure (he1) shows a constant presence of more than 10 mangroves throughout the entire monitoring campaign. Other structures show sporadic settlement events, followed by periods where amount slowly subside, and eventually disappear. Figure 3.14 shows mangrove counts and SBL height for three structures (Structures: he1, tw2 and 1). At all locations, deposition has taken place, showing an increase of around 35 cm relative to initial conditions. Average mangrove height increases at location he1.

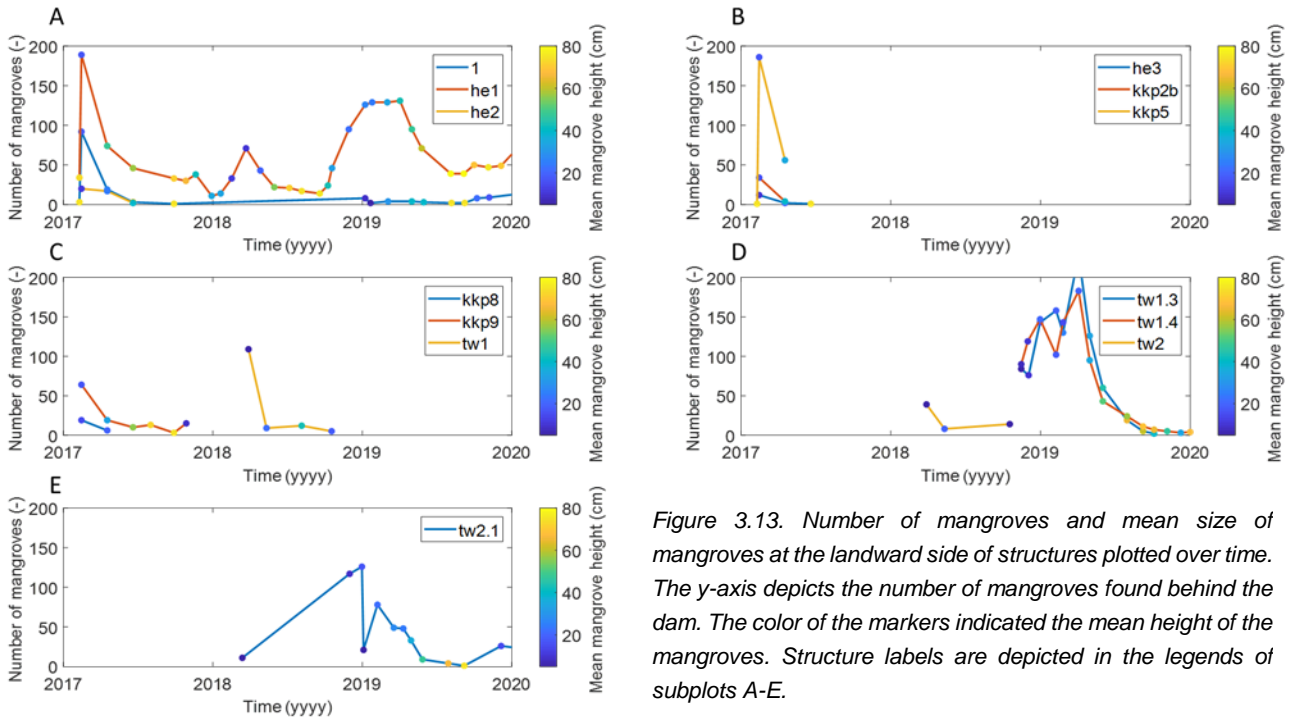


Figure 3.13. Number of mangroves and mean size of mangroves at the landward side of structures plotted over time. The y-axis depicts the number of mangroves found behind the dam. The color of the markers indicated the mean height of the mangroves. Structure labels are depicted in the legends of subplots A-E.

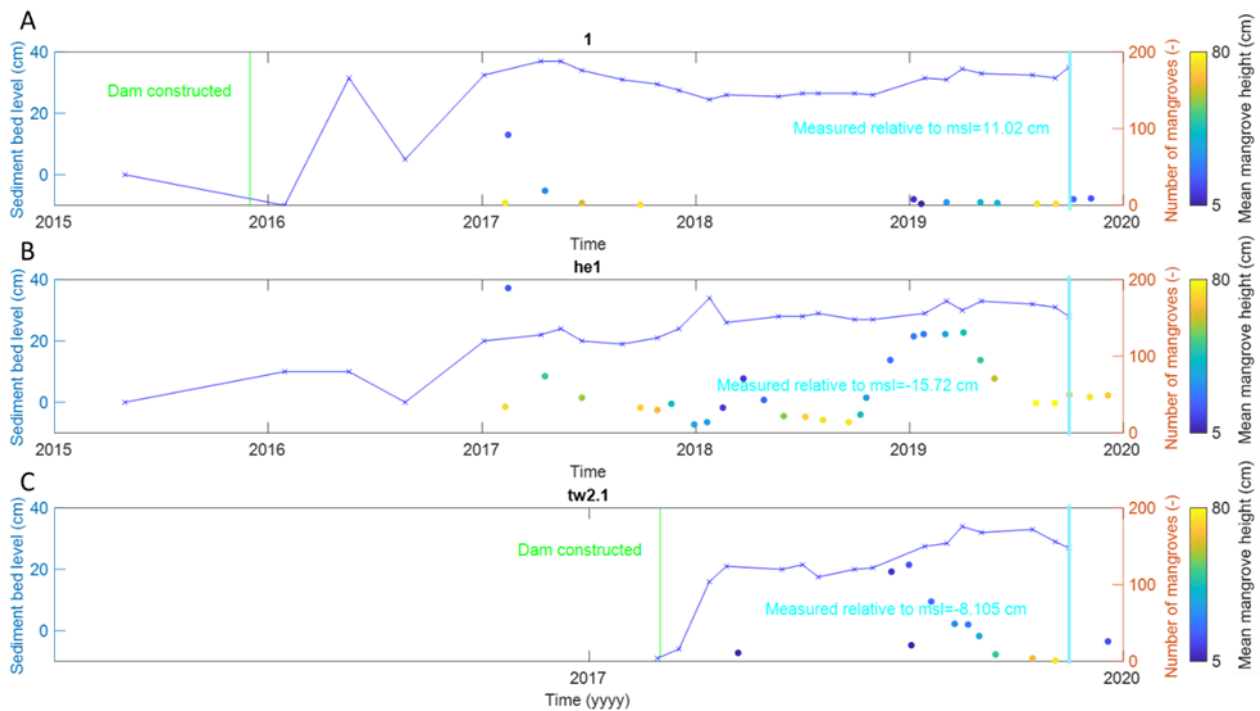


Figure 3.14. Left y-axis depicts sediment bed level averaged over associated poles, which indicates erosion or deposition with respect to start of the measurements. Right y-axis depicts the number of mangroves found behind the dam. The color of the markers indicated the mean height of the mangroves. Dam labels are depicted in the title of the subplot A-C.

4 Discussion

4.1 General

Finding effective methods to restore and preserve mangrove habitat remains relevant given their global decline (Thomas et al. 2017). In Demak, Java (Indonesia), the design and placement of permeable structures were geared towards creating suitable habitat for mangrove reestablishment by locally elevating SBL. This monitoring report summarizes the effectiveness of the permeable structures to counteract erosive forces that drive mangrove loss in Demak. Data shows that permeable structures trap sediment, elevate SBL and allow mangrove seedling establishment. However, overall sediment bed level rarely rose above mean sea level and mangroves did not develop beyond heights of sapling stage. This might be caused by high rates of subsidence in the research area (Chaussard et al. 2013a) combined with rapid degeneration and insufficient structural maintenance of the permeable structures.

4.2 Sediment bed level change

Overall, a lowering of SBL was observed in control locations (on average -8 cm) and an increase in SBL was detected behind the permeable structures (on average 20 cm). Generally, the largest increase occurred within the first 8 - 12 weeks after structure placement, after which increase in SBL slowed down. Similar trends are described by a study that monitored SBL behind permeable structures in Vietnam (Van Cuong et al. 2015a). In their study, Van Cuong et al. (2015a) show an increase of 30 cm behind structures in the first year, as opposed to control sites, where increase is less than 5cm. In the current study, SBL behind the permeable structures was strongly influenced by the state of the permeable structure. Below a certain level of structural integrity, the wave dampening function of the permeable structure possibly diminished to such an extent that erosion occurred, and the bed level declined. A second factor influencing changes in SBL is the elevation at which the permeable structures were initially placed. Generally, net lowering of SBL was observed at deeper locations (below -60 cm relative to MSL) and net increase in SBL was detected at shallow locations (above -20 cm relative to MSL). Increase in SBL correlated with depth for grid ($r^2 = 0.74$) and control ($r^2 = 0.86$) locations. Although control poles are slightly further from the shore than grid poles, these effects are expected to be minimal as grid and control poles are generally not more than 10 meters apart. Also, SBL measurements before and after placement of a structure, indicate that the structures have effect and that the effects are not only caused by differences in initial placement depth of control and grid poles. Variation in the data between different dams and locations can most likely be explained by local differences in wave and tidal forcing (Hu et al. 2017) and creek formation behind our permeable structures (*pers obs*). Finally, no correlation between deposition and the occurrence of the monsoon season was found.

The consolidation study (appendix D) revealed that likely sediment supply is not limiting sedimentation in the project area. At least, not during the monsoon period over which deposition next to the structures was measured. Initial consolidation is relatively fast (a 15 cm soft bed can accumulate in only 2 days). Probably, the strength that the accumulated sediment can attain, is of more importance for the final net sedimentation, by determining whether sediment can be picked up again after settling. Furthermore, the consolidation study indicated that average hydrodynamic conditions can limit consolidation of the bed by stirring up the sediment and bringing it into resuspension. We hypothesize that this effect is smaller at deeper sediment layers, as the lower layers in thick deposited layers will be better protected from hydrodynamics, hence consolidating more efficiently. The weaker sediment layer resulting from consolidation under average hydrodynamics will be more susceptible of being eroded at potential future eroding events, eventually resulting in limited net or no sedimentation. Net sedimentation may therefore depend on quiet hydrodynamic conditions for prolonged periods of time, or on the fast deposition of a thick layer of sediment that may be capable of protecting the underlying layers from the stirring effect of hydrodynamics.

4.3 Mangrove Recruitment

Besides increasing bed level and halting the coastal erosion process the aim of the permeable structures was to restore mangrove habitat and facilitate mangrove colonization. Although mangrove recruitment was observed behind several of the permeable dams, a full-grown forest has not developed during the project lifetime. Each year two recruitment events were recorded. Mangrove counts peaked at the same moment across all plots in December and in March. Generally, recruitment events started with massive seedling settlement, followed by a sharp decline in number of surviving plants. These patterns are more often observed in mangroves and salt marshes (Balke et al. 2011a, 2015).

The fact that mangrove recruitment was observed indicates that initially permeable structures created suitable conditions for mangrove colonization. Abiotic parameters such as inundation time, wave impact and bulk density determine mangrove establishment (Lewis 2005, van Bijsterveldt et al. 2020). However, established mangrove seedlings did not develop into full-grown trees, as they never exceeded 1 m in height. A possible hypothesis is that mangroves established behind the structures after initial sediment deposition raised the bed above MSL. Afterwards the combination of sediment consolidation, subsidence and erosion, lowered the bed below sea level again, sinking the already established mangroves below MSL as well (Figure 3.12 and Figure 4.3). This results in prolonged inundation time, which may cause their slow growth. Combined with low bulk density found behind the permeable structures, and mangroves roots anchoring to limited depths (Tomlinson 2019), conditions seem unfavourable for development of full-grown mangrove forests under the given hydraulic conditions.

4.4 Methodological

Methodological concerns related to the chosen monitoring method, such as measuring pole buoyancy and scouring, were systematically addressed. A force balance analysis, looking if PVC-measuring poles would either sink or “float” in conjunction with a subsiding landscape, indicated that the PVC measuring poles sink in with their surroundings and are not likely to float or being sucked into the mud. This implies that monitoring poles subside steadily with the bed, gradually sinking below mean sea level. Another uncertainty of the monitoring method is related to potential scouring around the PVC-measuring poles. Scouring has the potential to confound the SBL-results by incorrectly indicating a decrease in elevation. Especially results at deeper locations would be questionable, since scouring scales with depth (Scour manual, 1997). However, no signs of scour around the poles were ever observed in the field. Also, to avoid measuring in a scour hole next to the pole the bed level was measured at several distances from the measuring poles. The SBL eventually noted would be the average of these multiple measurements.

The change in SBL was monitored with respect to SBL at time of placement (T_0) of monitoring poles. As such, the method of monitoring does not distinguish between the processes that drive fluctuations in SBL, such as erosion, consolidation and deposition, as it solely measures the net effect (Equation 2-1). For example, quite often deposition events at monitoring poles were followed by a decline in SBL. It is in principle unclear if this decline is driven by erosion, consolidation or a combination of both processes. To overcome this lack of clarity, we executed a consolidation analysis of Demak sediment and conditions (5D).

During the 4-year monitoring campaign, depth of the permeable structures relative to mean sea level was measured once. This indicated that all structures were situated below mean sea level. Hence, the bed level behind the bed may not have risen above mean sea level for most structures. Under natural conditions mangroves inhabit areas in the upper part of the intertidal range, i.e. from mean sea level to mean high water (Smith, 1992). The structures being situated below mean sea level, could explain the limited mangrove settlement observed in the grid sites. For future monitoring campaigns of permeable structures, it is recommended to include more frequent measurements of bed level relative to mean sea level. By doing so, analysis of monthly variation in mangrove settlement can be linked to inundation period as an explanatory variable.

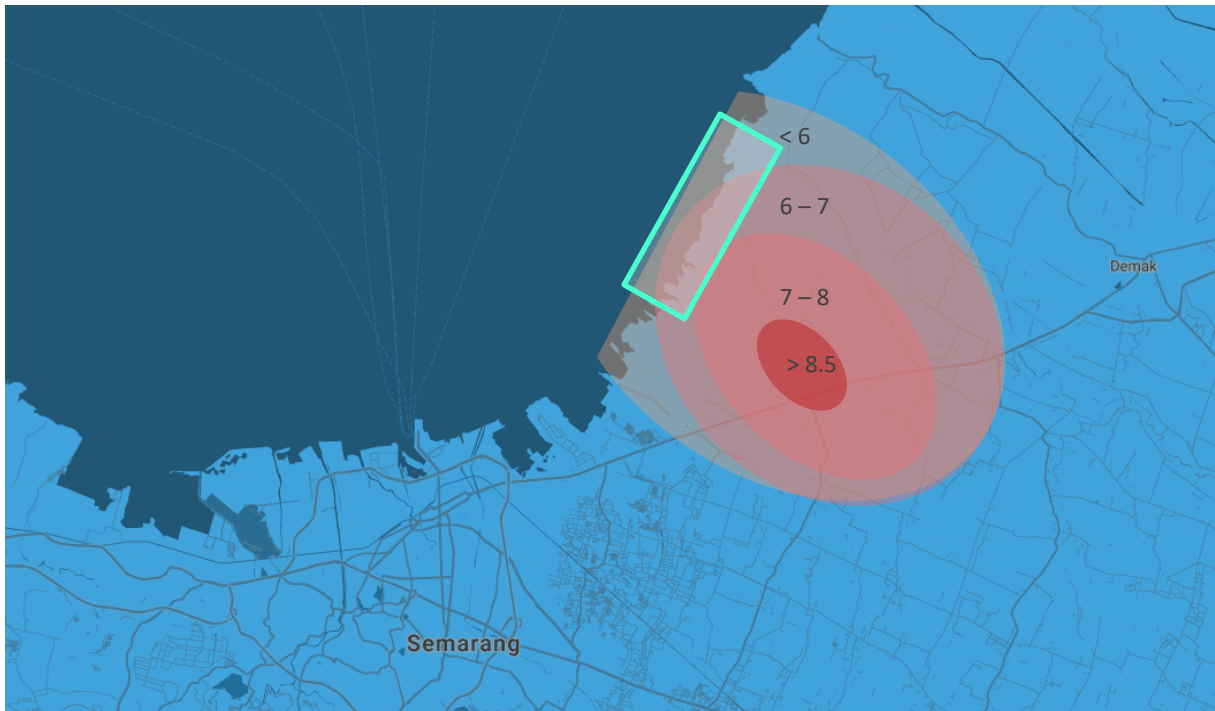


Figure 4.1. Map adopted from Yuwono et al. (2018), showing ground deformation (the red circles) in research area (indicated by the green box). Yearly subsidence rates are shown on the map in cm per year.

Ongoing subsidence in the area adds uncertainty in interpretation of the monitoring data. Observations on houses and bridges and data from water level loggers (under preparation) suggest that substantial subsidence occurs in the Demak coastal zone and that rates differ over the project area. Also, as water use still increases rapidly in the area subsidence may show a non-linear increase over the past years. Compaction is a common phenomenon in alluvial fine sediments and occurs under natural circumstances. Under natural compaction subsidence rates rarely exceed 1cm/year and rates are expected to be uniform over larger areas. Man-induced subsidence rates, however, can exceed 50 cm/year (Dolan & Grant, 1986, Kuehn, et al., 2010). Spatially, the most severe subsidence often coincides with the area with the largest lowering in ground water tables (Schmidt, 2002, Kuehn, et al., 2010). Semarang, the neighbouring city of Demak, is home to several industries that are large ground water extractors. Several locations in the city show severe signs of subsidence, exceeding rates of 13 cm/year (Chaussard et al. 2013a). The presence of industry and the similar geological characteristics of Demak may potentially result in similar subsidence rates (Figure 4.1). Several techniques have been used to report subsidence rates in Semarang and Demak (Andreas et al. 2019, Yastika et al. 2019) and subsidence in Demak is reported to reach rates of 8 cm annually (Yuwono et al. 2018).

Implications of subsidence for the interpretation of our monitoring data and for sedimentation behind the permeable structure are not straightforward. First, as relative sea level increases due to subsidence, larger waves are formed and bed shear stress increases which promotes resuspension, especially of newly deposited sediments. This may contribute to the gradual decline in net deposition rates behind the permeable structures and a to landward shift of the shoreline. Second, subsidence results in the creation of new accommodation space. However, if accommodation space increases, sedimentation may also increase if sediment availability is not limited and if there is sufficient transport capacity by currents and tides to distribute available sediment over the subsiding area (Angela et al. 2003). Behind the permeable structures a continuous and gradual increase in SBL is observed. This may be the infilling of the extra created accommodation space. Finally, subsidence may prevent consolidation of the sediment by reducing submergence time and thereby reducing potential for drainage and consolidation.

Unconsolidated sediment is more easily picked up by the waves and may not be optimal for mangrove development. Hence, structural integrity of the permeable structures to avoid resuspension of the sediment may have been even more important under subsiding conditions.

4.6 Variation in spatial characteristics



Figure 4.2. Map of the research area, the black lines represent the different locations of the structures. The foreshore is characterized by different geographical features, because of these large gradients differences in evolution can be encountered. The **A**, **B** and **D**: high wave exposure. **C**: large tidal volume inducing large current velocities and fringing mangroves. **E**: chenier present in the foreshore.

Results of the mixed model (Figure 3.4) strongly suggest that spatial variation in morphology and hydrodynamics are influencing SBL development behind and in front of the permeable structures. It is hypothesized that because of large gradients in morphological and hydrodynamic forces, differences in SBL development are encountered (Figure 3.2). Based on system understanding of the entire area, homogeneous areas are grouped as depicted in Figure 4.2. Morphological and hydrodynamics characteristics that influence the form and shape of the foreshore are the presence of cheniers (Figure 4.2 location E), being exposed to erosive waves (Figure 4.2 location A, B and D), fringing mangroves providing shelters (Figure 4.2 location C) and a large tidal volume inducing large current velocities (Figure 4.2 location C1). Abiotic characteristics, such as the presence of creeks and of a chenier, alter local wave conditions and sedimentation patterns. In fact, structures and cheniers could be interacting, having a cumulative effect on wave height reduction.

4.7 Conclusion

To conclude, this study showed that the permeable structures are effective at trapping sediment and mangroves colonization can take place behind the permeable structures. However, there is limited evidence that the seedlings can develop into healthy full-grown mangrove forests behind the structures. It is evident that permeable structures constitute an effective means to elevate SBL and to promote mangrove settlement. However, for Demak the permeable structures did not result in restoration of a mangrove greenbelt as envisioned during project initiation. The 4 years of monitoring and analysis helped with writing a conceptual framework that untangles the different process taking place simultaneously and how each of them affects the capturing of sediment and settlement of mangroves. As shown in Figure 4.3 these processes are: accretion, mangrove recruitment, dam degeneration, consolidation, and subsidence. The framework set forth in the figure explains that the structures result in sedimentation and eventually mangrove seedling settlement. However, mangrove growth is severely impeded because erosive forces increase as SBL is lowered because of subsidence and the degeneration of the permeable structures.

These insights underscore the importance of firstly, ensuring year-round structural integrity. Secondly, it reaffirms the need to understand system scale processes in order to effectively restore mangrove habitat in a subsiding landscape. Lack of trustworthy and quantitative information on levels of subsidence in Demak at the onset of the project hampered implementation and evaluation of the results.

There are many publications that show subsidence occurs in Semarang (Chaussard et al. 2013b, Husnayaen et al. 2018, Yuwono et al. 2018, 2019, Andreas et al. 2019, Prasetyo et al. 2019, Yastika et al. 2019), but no data on how this translates to subsidence in Demak was available at the start of this project. Nowadays, GPS derived data is available that provides trustworthy measurements on subsidence in Demak (Yuwono et al. 2018). Sedimentation can keep up with certain levels of relative sea level rise, but if relative sea level rise is too sudden or fast the amount of available sediment or the amount of sediment that can be suspended in the water column and that can be transported by the tides can all become limiting factors (Woodroffe et al. 2016). In addition, the relative sea level rise that mangroves can cope with is also limited.

Finally, the levels of subsidence warranted for much higher levels of maintenance of permeable structures. Overall, it is assumed that without high rates of subsidence and subsequent increase in accommodation space, permeable structures offer a viable method to restore mangrove habitats along eroding coastlines. The structures show that SBL can reach levels near MSL, and that suitable conditions are met for mangrove recruitment. Paying attention to a proper analysis of the natural system and the environmental boundary conditions is required. Permeable structures are considered most feasible for areas with low wave impact, to limit maintenance of structures and to allow sufficient damping of waves by the structure. As tidal movement is needed for sediment transport, a moderate tidal amplitude is beneficial. Overall, permeable structures represent an adaptive and relatively low-tech measure, and thus may constitute a means for coastal communities to cope with or delay coastal erosion. However, crucial for a sustainable future for coastal communities in Demak is that mitigative measures to address the root cause of subsidence, are also implemented. If restoration and monitoring activities are taking place in an area that is subsiding, mapping of vertical displacement is crucial. It helps with understanding the sediment dynamics in the system, as it elucidates if erosive forces are increasing and if sediment supply becomes a limiting factor.

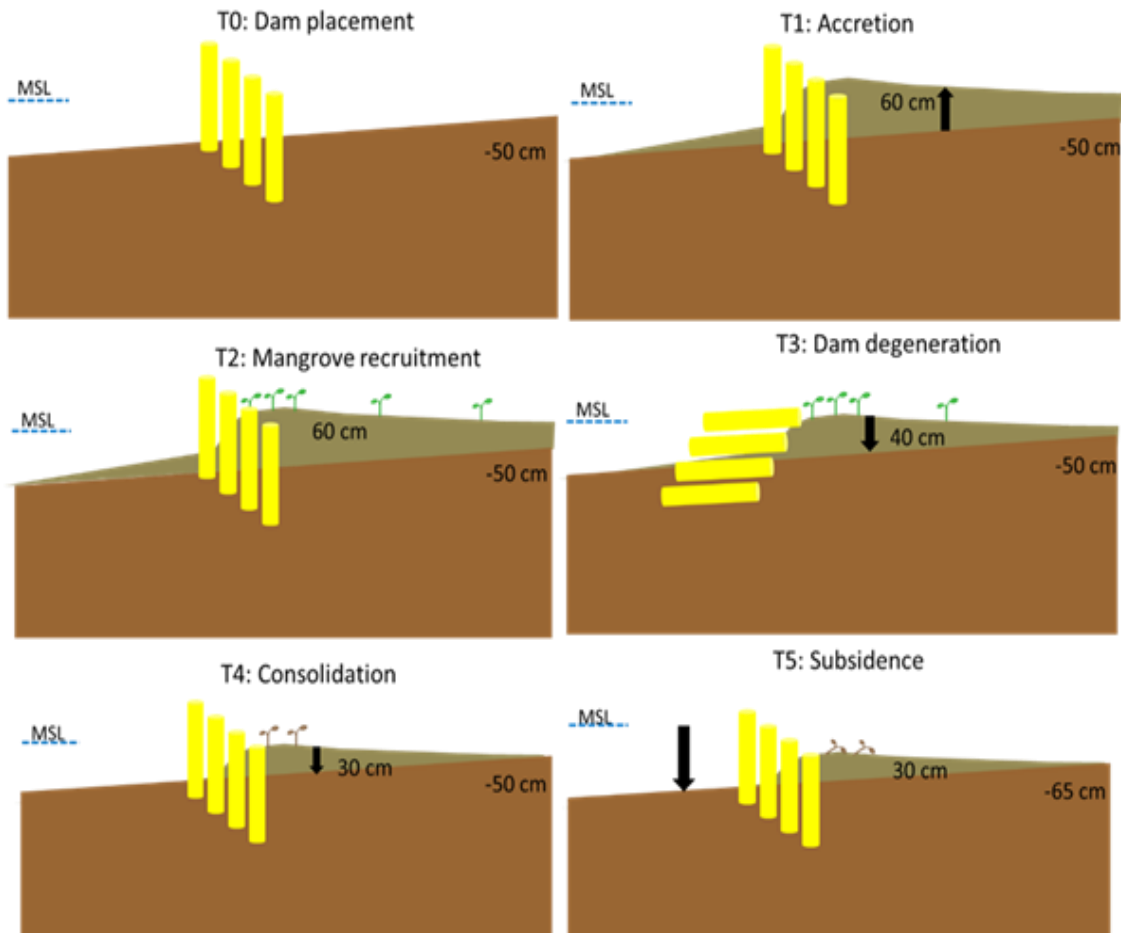


Figure 4.3. A Conceptual framework describing the development of SBL and mangrove recruitment behind the structures influenced by dam degeneration, subsidence and consolidation. T_0 : Placement of permeable structure. T_1 : Sedimentation occurs behind the permeable structure. For example, a total of 60 cm of fine sediments is deposited. T_2 : The elevated sediment bed level is ideal for the settlement of mangrove seedlings. Seedlings start to grow. T_3 : The permeable structure degenerates and is no longer able to maintain proper hydraulic conditions to capture and stabilize sediment. The elevation drops to 40 cm, as the deposited sediment is brought into resuspension and transported out of the area. T_4 : The freshly deposited sediment consolidates. The sediment bed level drops to 30 cm's. Elevation becomes too low and submergence time too long for mangrove settlement and growth of established mangroves. T_5 : Subsidence is ongoing. The entire area sinks below mean sea level and emergence time is too high for mangrove establishment and survival.

- Abidin, H. Z., H. Andreas, I. Gumilar, T. P. Sidiq, and Y. Fukuda. 2013. Land subsidence in coastal city of Semarang (Indonesia): Characteristics, impacts and causes. *Geomatics, Natural Hazards and Risk* 4:226–240.
- Adams, J. B., and L. R. D. Human. 2016. Investigation into the mortality of mangroves at St. Lucia Estuary. *South African Journal of Botany* 107:121–128.
- Andreas, H., H. Zainal Abidin, I. Gumilar, T. Purnama Sidiq, D. Anggreni Sarsito, and D. Pradipta. 2019. On the acceleration of land subsidence rate in Semarang City as detected from GPS surveys. *E3S Web of Conferences* 94.
- Angela, L., D. W. J. Bosence, K. D. Church, W. J. Dan, S. S. Flint, D. Kevin, J. A. Howell, A. John, and R. C. L. Wilson. 2003. *The sedimentary record of sea-level change*. Cambridge University Press.
- Balke, T., T. Bouma, E. Horstman, E. Webb, P. Erftemeijer, and P. Herman. 2011a. Windows of opportunity: thresholds to mangrove seedling establishment on tidal flats. *Marine Ecology Progress Series* 440:1–9.
- Balke, T., T. J. Bouma, E. M. Horstman, E. L. Webb, P. L. A. Erftemeijer, and P. M. J. Herman. 2011b. Windows of opportunity: Thresholds to mangrove seedling establishment on tidal flats. *Marine Ecology Progress Series*.
- Balke, T., T. J. Bouma, E. M. Horstman, E. L. Webb, P. L. A. Erftemeijer, and P. M. J. Herman. 2011c. Windows of opportunity: Thresholds to mangrove seedling establishment on tidal flats. *Marine Ecology Progress Series* 440:1–9.
- Balke, T., A. Swales, C. E. Lovelock, P. M. J. Herman, and T. J. Bouma. 2015. Limits to seaward expansion of mangroves: Translating physical disturbance mechanisms into seedling survival gradients. *Journal of Experimental Marine Biology and Ecology* 467:16–25.
- Balke, T., E. L. Webb, E. van den Elzen, D. Galli, P. M. J. Herman, and T. J. Bouma. 2013. Seedling establishment in a dynamic sedimentary environment: A conceptual framework using mangroves. *Journal of Applied Ecology* 50:740–747.
- Barbier, E. B. 2016. The protective service of mangrove ecosystems: A review of valuation methods. *Marine Pollution Bulletin* 109:676–681.
- Bates, D., M. Mächler, B. Bolker, and S. Walker. 2015. Fitting Linear Mixed-Effects Models Using lme4 | Bates | *Journal of Statistical Software*. *Journal of Statistical Software* 67:1–48.
- Bennett, E. L., and C. J. Reynolds. 1993. The value of a mangrove area in Sarawak. *Biodiversity and Conservation* 2:359–375.
- van Bijsterveldt, C. E. J., B. K. van Wesenbeeck, D. van der Wal, N. Afiati, R. Pribadi, B. Brown, and T. J. Bouma. 2020. How to restore mangroves for greenbelt creation along eroding coasts with abandoned aquaculture ponds. *Estuarine, Coastal and Shelf Science* 235:106576.
- Borsje, B. W., B. K. van Wesenbeeck, F. Dekker, P. Paalvast, T. J. Bouma, M. M. van Katwijk, and M. B. de Vries. 2011. How ecological engineering can serve in coastal protection.
- Brunier, G., N. Gratiot, E. Anthony, and A. Gardel. 2019. Exceptional rates and mechanisms of muddy shoreline retreat following mangrove removal.
- Carlton, J. M. 1974. Land-building and Stabilization by Mangroves. *Environmental Conservation* 1:285–294.
- Chaussard, E., F. Amelung, H. Abidin, and S. H. Hong. 2013a. Sinking cities in Indonesia: ALOS PALSAR detects rapid subsidence due to groundwater and gas extraction. *Remote Sensing of Environment* 128:150–161.
- Chaussard, E., F. Amelung, H. Abidin, and S. H. Hong. 2013b. Sinking cities in Indonesia: ALOS PALSAR detects rapid subsidence due to groundwater and gas extraction. *Remote Sensing of Environment* 128:150–161.
- Clough, B. F. 1982. *Mangrove ecosystems in Australia: structure, function and management*. Proceedings.
- Coe, A. L., D. W. J. Bosence, K. D. Church, S. S. Flint, J. A. Howell, and R. C. L. Wilson. 2003. *The Sedimentary Record of Sea-Level Change*. Page (A. L. Coe, Ed.). The press syndicate of the university of cambridge, Cambridge, United Kingdom.
- Van Cuong, C., S. Brown, H. H. To, and M. Hockings. 2015a. Using Melaleuca fences as soft coastal engineering for mangrove restoration in Kien Giang, Vietnam. *Ecological Engineering* 81:256–265.

- Van Cuong, C., S. Brown, H. H. To, and M. Hockings. 2015b. Using *Melaleuca* fences as soft coastal engineering for mangrove restoration in Kien Giang, Vietnam. *Ecological engineering* 81:256–265.
- Dahdouh-Guebas, F., L. P. Jayatissa, D. Di Nitto, J. O. Bosire, D. Lo Seen, and N. Koedam. 2005, June 21. How effective were mangroves as a defence against the recent tsunami? *Cell Press*.
- Defries, R. S., T. Rudel, M. Uriarte, and M. Hansen. 2010. Deforestation driven by urban population growth and agricultural trade in the twenty-first century. *Nature Geoscience* 3:178–181.
- Dijkema, K. S., A. S. Kers, and W. E. Van Duin. 2010. Salt marshes : applied long-term monitoring salt marshes. Pages 35–40 *Wadden Sea Ecosystem* no. 26.
- Donato, D. C., J. B. Kauffman, D. Murdiyarto, S. Kurnianto, M. Stidham, and M. Kanninen. 2011. Mangroves among the most carbon-rich forests in the tropics. *Nature Geoscience* 4:293–297.
- Eong, O. J. 1993. Mangroves - a carbon source and sink. *Chemosphere* 27:1097–1107.
- Friess, D. A., K. Rogers, C. E. Lovelock, K. W. Krauss, S. E. Hamilton, S. Y. Lee, R. Lucas, J. Primavera, A. Rajkaran, and S. Shi. 2019. The State of the World's Mangrove Forests: Past, Present, and Future. *Annual Review of Environment and Resources* 44:89–115.
- Galloway, D. L., and T. J. Burbey. 2011. Review: Regional land subsidence accompanying groundwater extraction. *Hydrogeology Journal* 19:1459–1486.
- Gedan, K. B., M. L. Kirwan, E. Wolanski, E. B. Barbier, and B. R. Silliman. 2010. The present and future role of coastal wetland vegetation in protecting shorelines : answering recent challenges to the paradigm. *Climate change*.
- Gedan, K. B., M. L. Kirwan, E. Wolanski, E. B. Barbier, and B. R. Silliman. 2011, May. The present and future role of coastal wetland vegetation in protecting shorelines: Answering recent challenges to the paradigm.
- Gilman, E. L., J. Ellison, N. C. Duke, and C. Field. 2008. Threats to mangroves from climate change and adaptation options: A review.
- Hossain, M. D., and A. A. Nuruddin. 2016. Soil and mangrove: A review. *Journal of Environmental Science and Technology* 9:198–207.
- Hu, Z., P. Yao, D. Van Der Wal, and T. J. Bouma. 2017. Patterns and drivers of daily bed-level dynamics on two tidal flats with contrasting wave exposure. *Scientific Reports* 7:1–9.
- Husnayaen, A. B. Rimba, T. Osawa, I. N. S. Parwata, A. R. As-syakur, F. Kasim, and I. A. Astarini. 2018. Physical assessment of coastal vulnerability under enhanced land subsidence in Semarang, Indonesia, using multi-sensor satellite data. *Advances in Space Research* 61:2159–2179.
- Kamali, B., and R. Hashim. 2011. Mangrove restoration without planting. *Ecological Engineering* 37:387–391.
- Kodikara, K. A. S., N. Mukherjee, L. P. Jayatissa, F. Dahdouh-Guebas, and N. Koedam. 2017. Have mangrove restoration projects worked? An in-depth study in Sri Lanka. *Restoration Ecology* 25:705–716.
- Kondolf, G. M., Z. K. Rubin, and J. T. Minear. 2014. Dams on the Mekong: Cumulative sediment starvation. *Water Resources Research* 50:5158–5169.
- Lewis III, R. R., and M. J. Marshall. 1998. Principles of successful restoration of shrimp aquaculture ponds back to mangrove forests. *Aquaculture '98 Book of Abstracts*:327.
- Lewis III, R. R., E. C. Milbrandt, B. Brown, K. W. Krauss, A. S. Rovai, J. W. Beever III, and L. L. Flynn. 2016. Stress in mangrove forests: Early detection and preemptive rehabilitation are essential for future successful worldwide mangrove forest management. *Marine Pollution Bulletin* 109:764–771.
- Lewis, R. R. 2001. Mangrove Restoration - Costs and Benefits of Successful Ecological Restoration. *Mangrove Valuation Workshop*:4–8.
- Lewis, R. R. 2005. Ecological engineering for successful management and restoration of mangrove forests. *Ecological Engineering* 24:403–418.
- Lovelock, C. E., D. A. Friess, and K. W. Krauss. 2015. the vulnerability of Indo-Paci & c mangrove forests to sea-level rise.
- Mazda, Y., M. Magi, H. Nanao, M. Kogo, T. Miyagi, N. Kanazawa, and D. Kobashi. 2002. Coastal erosion due to long-term human impact on mangrove forests. *Wetlands Ecology and Management* 10:1–9.
- Mcdonald, T., G. D. Gann, J. Jonson, and K. W. Dixon. 2016. About the Society for Ecological Restoration. *Communications Standards*:427–437.
- Mehta, A. J. 1986. Characterization of cohesive sediment properties and transport processes in estuaries. *Estuarine cohesive sediment dynamics. Proc. workshop, Tampa, 1984*:290–325.
- Montgomery, J., K. Bryan, E. Horstman, and J. Mullarney. 2018. Attenuation of Tides and Surges by Mangroves: Contrasting Case Studies from New Zealand. *Water* 10:1119.

- Nathan, A. J., and A. Scobell. 2012. How China sees America.
- Nicholls, R. J., F. M. J. Hoozemans, and M. Marchand. 1999. Increasing flood risk and wetland losses due to global sea-level rise: Regional and global analyses. Page Global Environmental Change.
- Ola, A., S. Schmidt, and C. E. Lovelock. 2018. The effect of heterogeneous soil bulk density on root growth of field-grown mangrove species. *Plant and Soil* 432:91–105.
- Ostendorp, W., C. Iseli, M. Krauss, P. Krumscheid-Plankert, J. L. Moret, M. Rollier, and F. Schanz. 1995. Lake shore deterioration, reed management and bank restoration in some Central European lakes. *Ecological Engineering* 5:51–75.
- Paryanti, S. 2006. National Aquaculture sector overview. Indonesia. National Aquaculture sector overview fact sheets. FAO Fisheries and Aquaculture Department. Rome.
- Polidoro, B. A., K. E. Carpenter, L. Collins, N. C. Duke, A. M. Ellison, C. Joanna, E. J. Farnsworth, E. S. Fernando, K. Kathiresan, N. E. Koedam, S. R. Livingstone, T. Miyagi, G. E. Moore, V. N. Nam, and J. E. Ong. 2010. The Loss of Species : Mangrove Extinction Risk and Geographic Areas of Global Concern 5.
- Prasetyo, Y., H. S. Firdaus, and Diyanah. 2019. Land Subsidence of Semarang City Using Permanent Scatterer Interferometric Synthetic Aperture Radar (Ps-Insar) Method in Sentinel 1a between 2014-2017. *IOP Conference Series: Earth and Environmental Science* 313.
- Quartel, S., A. Kroon, P. G. E. F. Augustinus, P. Van Santen, and N. H. Tri. 2007. Wave attenuation in coastal mangroves in the Red River Delta, Vietnam. *Journal of Asian Earth Sciences* 29:576–584.
- Richards, D. R., and D. A. Friess. 2015. Rates and drivers of mangrove deforestation in Southeast Asia, 2000–2012. *Proceedings of the National Academy of Sciences* 113:344–349.
- Rubin, Z. K., G. M. Kondolf, and P. A. Carling. 2015. Anticipated geomorphic impacts from Mekong basin dam construction. *International Journal of River Basin Management* 13:105–121.
- Spalding, J. 2011. *World Atlas of Mangroves*.
- Thampanya, U., J. E. Vermaat, and C. M. Duarte. 2002. Colonization success of common Thai mangrove species as a function of shelter from water movement. *Marine Ecology Progress Series* 237:111–120.
- Thomas, N., R. Lucas, P. Bunting, A. Hardy, A. Rosenqvist, and M. Simard. 2017. Distribution and drivers of global mangrove forest change, 1996-2010. *PLoS ONE* 12:1–14.
- Tomlinson, P. B. 2019. The botany of mangroves content page.
- Tonneijck, F., H. Winterwerp, B. van Weesenbeeck, R. Bosma, D. Debrot, Y. R. Noor, and T. Wilms. 2015. Building with Nature Indonesia Securing Eroding Delta Coastlines:1–65.
- Toorman, E. A., E. Anthony, P. G. E. F. Augustinus, A. Gardel, N. Gratiot, O. Homenauth, N. Huybrechts, J. Monbaliu, K. Moseley, and S. Naipal. 2018. Interaction of Mangroves, Coastal Hydrodynamics, and Morphodynamics Along the Coastal Fringes of the Guianas. Pages 429–473.
- Valiela, I., J. L. Bowen, and J. K. York. 2001. Mangrove Forests: One of the World's Threatened Major Tropical Environments. *BioScience* 51:807.
- del Valle, A., M. Eriksson, O. A. Ishizawa, and J. J. Miranda. 2019. Mangroves Protect Coastal Economic Activity from Hurricanes. *Proceedings of the National Academy of Sciences of the United States of America*:1–6.
- Vuik, V., B. W. Borsje, P. W. J. M. Willemsen, and S. N. Jonkman. 2019. Salt marshes for flood risk reduction: Quantifying long-term effectiveness and life-cycle costs. *Ocean and Coastal Management* 171:96–110.
- Wesenbeeck, B. K. Van, T. Balke, P. Van Eijk, F. Tonneijck, and H. Y. Siry. 2015. Aquaculture induced erosion of tropical coastlines throws coastal communities back into poverty. *Ocean and Coastal Management* 116:466–469.
- Winterwerp, H., B. Van Wesenbeeck, J. Van Dalftsen, F. Tonneijck, A. Astra, S. Verschure, and P. Van Eijk. 2014. A sustainable solution for massive coastal erosion in Central Java : Towards Regional Scale Application of Hybrid Engineering:45.
- Winterwerp, J. C., W. G. Borst, and M. B. de Vries. 2005. Pilot Study on the Erosion and Rehabilitation of a Mangrove Mud Coast. *Journal of Coastal Research* 212:223–230.
- Woodroffe, C. D., K. Rogers, K. L. McKee, C. E. Lovelock, I. A. Mendelsohn, and N. Saintilan. 2016. Mangrove Sedimentation and Response to Relative Sea-Level Rise. *Annual Review of Marine Science* 8:243–266.
- Wyrski, K. 1961. *NAGA REPORT Volume 2 Scientific Results*:195.
- Yastika, P. E., N. Shimizu, and H. Z. Abidin. 2019. Monitoring of long-term land subsidence from 2003 to 2017 in coastal area of Semarang, Indonesia by SBAS DInSAR analyses using Envisat-ASAR, ALOS-PALSAR, and Sentinel-1A SAR data. *Advances in Space Research* 63:1719–1736.

Yuwono, B. D., Y. Prasetyo, and L. J. F. Islama. 2018. Investigation of Potential Landsubsidence using GNSS CORS UDIP and DinSAR, Sayung, Demak, Indonesia. IOP Conference Series: Earth and Environmental Science 123.

Yuwono, B. D., S. Subiyanto, A. S. Pratomo, and N. Najib. 2019. Time series of land subsidence rate on coastal demak using gnss cors udip and dinsar. E3S Web of Conferences 94:2–6.

A Appendix: Locations of PVC measuring poles and permeable structures.

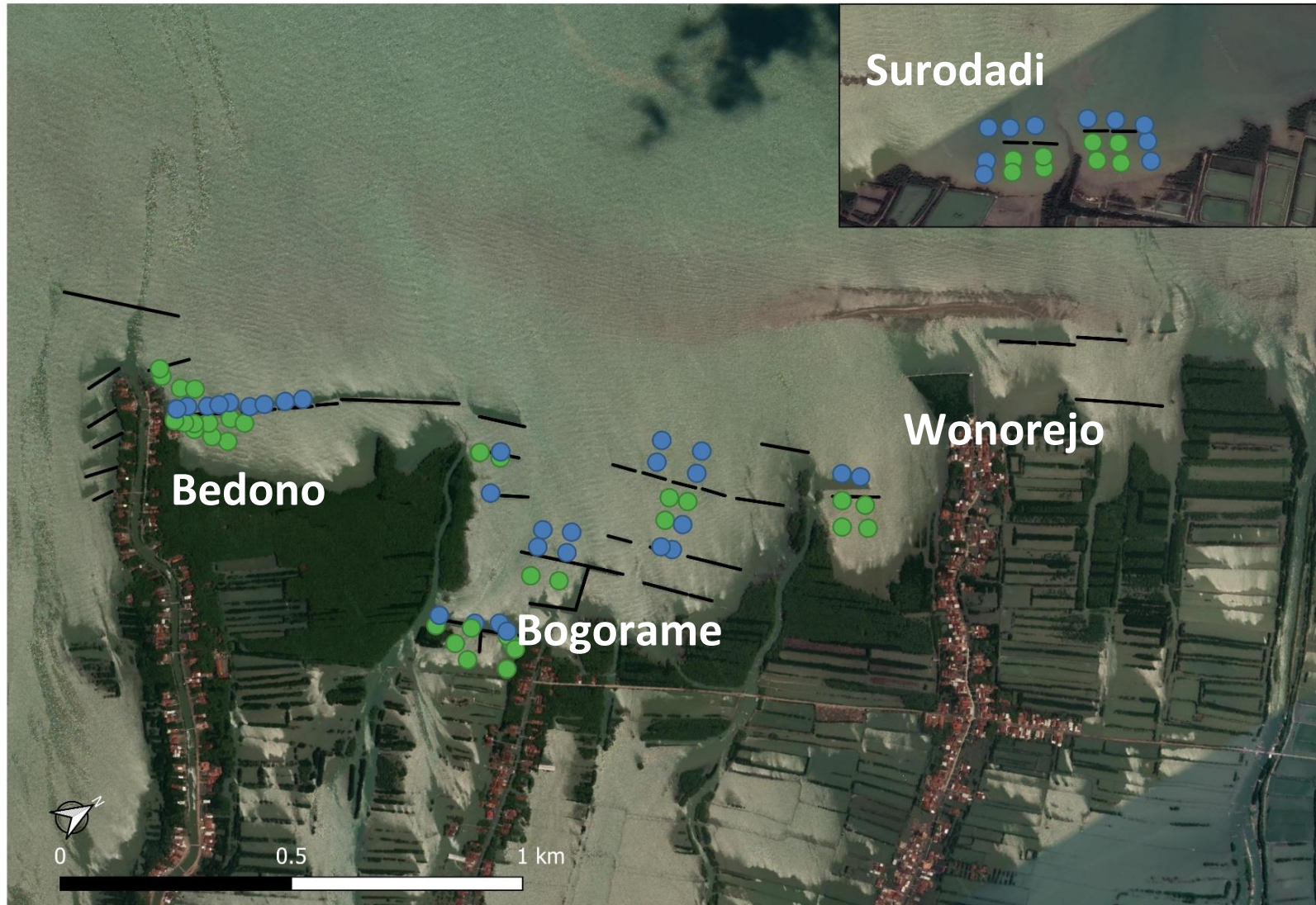


Figure A.1 Satellite image of the research area. The green and blue dots represent the locations of the PVC-measuring poles. Green dots correspond to grid measuring poles, and blue dots to control measuring poles. The black lines represent the permeable structures. The 4 different villages within the research area are shown. Surodadi, is 2km further north along the coast line. Parallel to the coastline, a chenier is clearly visible, just off the coast of Wonorejo.

B Appendix: Locations of single measuring event in September of 2019

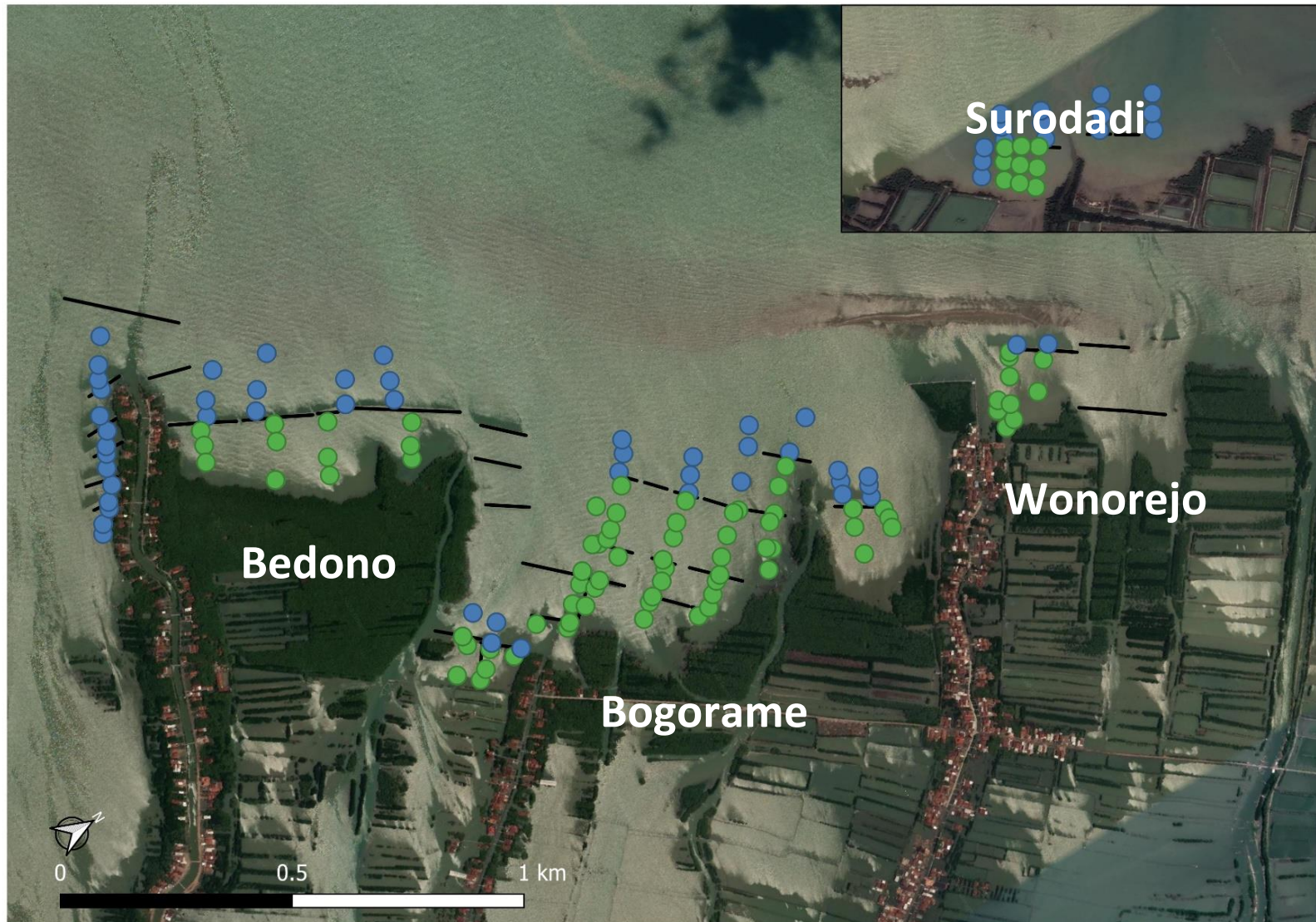


Figure B.1 Satellite image of the research area. The green and blue dots represent the locations of the measurements. Green dots correspond to locations behind structures, blue dots represent locations in front of structures. These measurements were used for the kriging, sbl monitoring and fluid mud monitoring. The black lines represent the permeable structures. The 4 different villages within the research area are shown. Surodadi, is 2km further north along the coast line.

C The state of permeable structure



Figure C.5.1. Four pictures of structures, each having been given a different qualitative state. The structure in **A** has a state of 1, nearly the entire structure is gone. The remainder of the structure is expected to have no significant effect on wave dissipation. The structure in **B** has a state of 3, it still has horizontal and vertical beams, however is lacking in brushwood. The structure in **C** has a state of 4, large beams are still present, but part of the brushwood has disappeared and some of the vertical beams are slanted. The structure in **D** has a state of 5, i.e. pristine. All brushwood is still present, and all large vertical and horizontal beams are undamaged.

D Summary of consolidation analysis

Authors: Miguel de Lucas, Jip Koster, Amrit Cado, Alejandra Gijon Mancheno, Bob Smits, Silke Tas, Celine van Bijsterveldt, Han Winterwerp, Peter Herman, Bregje van Wesenbeeck

D.1 Introduction

In this appendix we present the development and the results of a fine sediment settling and consolidation model, typically called consolidation model. The model feeds on the results from an extensive laboratory campaign performed by [Biomanco](#) and Deltares staff to Demak sediment, and on field data obtained at the project site by Biomanco and support personnel of Deltares. The purpose of this work is two-fold.

1. The objective is to set up a consolidation model that can be used in future projects on the area, or by the community of researchers around the project.
2. The second objective is to produce a first set of model results, providing some insight on consolidation that would help with the interpretation of the sedimentation results as presented in this report.

In particular, by using this model we aim to indicate the time and the length scales involved in consolidation at the Demak project site in an approximate manner, as well as to evaluate the relative importance of each of the factors contributing to sedimentation (e.g. deposition, consolidation, and erosion) at the study site.

In the first section of this appendix we discuss the methodology for developing the model, including some aspects of the laboratory campaign and field campaign contributing to it. Later in the results section we provide information on how the laboratory results were used as input for the model, on the hydrodynamic and sediment conceptual picture arising from the field measurements, and finally on the results of the model when run for the conceptual picture as derived from the field.

D.2 Methodology

In this section we briefly describe all the methodology involved in the development and execution of the consolidation analysis. The consolidation model had a central role. The laboratory experiments and field measurements were used for its calibration and settings selection and are therefore included in this section as well.

D.2.1 Laboratory tests

Laboratory experiments were performed in a set of so-called settling and consolidation columns. These are made of PVC, are transparent, and are typically 1 m high and 0.1 m in diameter. Essentially, the experiments consist of filling the settling and consolidation columns with a homogenous mixture of mud and water. Shortly after the test starts, two layers form: a layer of water on top and a layer of sediment in the bottom. With time, the interface between mud and water lowers, following the densification of the mud layer. By monitoring this dropping mud-water interface, we can determine the so-called consolidation parameters. These parameters are necessary to model consolidation, as they in fact define the consolidation behavior of mud. The parameters are:

- the fractal dimension n_f ,
- the permeability parameter K_k ,
- the effective stress parameter K_p ¹.

A necessary condition for being able to derive consolidation parameters from a consolidation test is that the mud-water mixture settles initially. This means that the initial sediment concentration should be low enough to obtain a suspension. In other words, the initial sediment concentration should be low enough not to have a bed from $t=0$. For details on how the consolidation parameters were obtained, the reader

¹ Note that these consolidation parameters are associated to a specific consolidation model, as will be explained in section 1.3.

is referred to the separate report “Soil Properties Demak” developed within the framework of the current project in a collaborative effort with Biomanco. For a detailed overview of the consolidation parameters and the theory behind them, the reader is referred to Merckelbach and Kranenburg (2004), or otherwise to Winterwerp and van Kesteren (2004) for a more general and applicable description of them.

Consolidation experiments are not only useful to derive consolidation parameters per se. They also provide data (other than the lowering mud-water interface) that is useful to validate the model results. This validation of the model results is accomplished by direct comparison of the bulk density profiles as measured at the end of laboratory tests, with these computed by the model. To measure the bulk density profiles at the end of laboratory tests, we used a UHCM (Ultrasonic High Concentration Meter). Essentially this is an acoustic probe that estimates bulk density by measuring the attenuation of an acoustic beam between two small electrodes. Details on this type of measurements, including calibration, can also be found at the separate report “Soil Properties Demak”.

D.2.2 Field observations

Throughout the several projects conveying at our study site (ours, but also Biomanco), many measuring campaigns took place. These all had independent research goals. Yet, some of the parameters measured in these campaigns are useful to understand and characterize consolidation dynamics in the study area. In particular, data derived from sediment trap and hydrodynamic measurements by Biomanco, and from the bulk density profile measurements by Deltares. The first are described in the PhD thesis by Gijon Mancheno, “Mangrove restoration using brushwood structure” (2020) and are used as boundary conditions for the consolidation model (e.g. sediment input, but also currents, waves and water depth). The second were reported at the MSc thesis from WUR “The effect of permeable structures on spatial sediment dynamics and mangrove reoccurrence” (2019) by the Deltares intern Jip Koster and are used as one extra observation in our consolidation study. For clarity, please note that the field observations will be split into two different sections when reported at the results section. The field measurements from Biomanco, being input for our model, will be reported before the model results. The field measurements by our intern will be reported subsequently and also before the model results, as they can certainly help with interpreting the model output.

D.2.3 Model

For this study we used a 1DV consolidation model based in the equations of Merckelbach and Kranenburg (2004) and developed for Deltares by Winterwerp and Uittenbogaard. The equations of Merckelbach and Kranenburg are just a simplified version of the Gibson consolidation equation (1958), following the assumption of a consolidating bed being self-similar. This model has been used in several peer-reviewed articles over settling and consolidation of mud (Winterwerp, 2002 & 2006). Essentially the model makes use of a set of parameters to reproduce the consolidation behavior of mud. These are the consolidation parameters, as introduced in section 1.2. Once the model is fed with its consolidation parameters, it can predict consolidation time and amount under a set of boundary conditions (hydrodynamic forcing, water depth, initial sediment concentration, etc).

This model is known to exhibit deviations from reality for large initial sediment thicknesses (in the order of magnitude of 1 m or more, approximately), but these are likely not to occur in the current project, justifying the choice of the modeling platform.

D.3 Results

D.3.1 Input to consolidation model I: laboratory tests with low initial sediment concentration

Multiple settling and consolidation experiments were performed to obtain the consolidation parameters. All the details associated to each of the experiments, as well as the detailed procedures and calculations for obtaining all parameters, are to be found at “Soil Properties Demak”. From all the executed tests, only one yielded a bulk density of 1350 kg/m³ in the lower layer (see again “Soil Properties Demak”), which is similar to what we observed in the field over the uppermost 20 cm of freshly deposited beds (see section 2.4. “in-situ bulk density profiles”). This was column C1, whose associated consolidation parameters are given in Table App D-1. The reasons why only one of our laboratory tests yielded bulk densities equivalent to these observed in the field cannot be determined. It may be related to a variety of reasons, including sediment structure and experimental procedure. The consolidation parameters as obtained from the laboratory of column C1, the only test yielding in-situ bulk densities, are used as direct input for the model.

Table App D-1. Selected set of consolidation parameters, following from consolidation tests.

Column	c (g/l)	K_r (m/s)	n_f (-)	K_p (Pa)
C1	97.1	$1.5 \cdot 10^{-12}$	2.63	$5.9 \cdot 10^5$

The acquisition of the bulk density profile of a bed resulting from a laboratory test enables us to validate a set of consolidation parameters. This is done by running the model for the selected set of parameters and for the same initial conditions as in the laboratory (sediment concentration and initial mud-water mixture height). Output of the model is compared with the bulk density measurements. Fig D-1 shows the comparison between the model results when adopting C1 settings and direct laboratory measurements at column C1. The model manages to reproduce the equilibrium bulk density profile to an acceptable degree. Multiple other model runs still with the C1 consolidation parameters but to the initial conditions of other laboratory tests from these discussed in “Soil Properties Demak” were also executed and resulted in good agreement between model results and measurements as well but are left outside this appendix for the sake of synthesis. Therefore, we conclude that the model, when based on C1 settings, can reproduce equilibrium bulk density profiles for a range of initial concentrations that in general do not exceed the concentrations in the field.

As for the equilibrium time for consolidation, we also compared equilibrium time from the model and from laboratory experiments. For example, in the laboratory the consolidation experiment C1 reached a near equilibrium height approximately at around $2 \cdot 10^5$ s, which is 2.3 days (see “Soil Properties Demak”), whereas the model predicts equilibrium somewhere around 3440 min, which is again approximately 2.3 days. Thus, not only the equilibrium bulk density profile is well predicted, but also the time in which equilibrium is reached is predicted within a 5% margin of error. The latter is again only valid for the range of initial concentrations verified via the execution of laboratory tests (i.e. up to 90 g/l). The model therefore delivers accurate predictions for conditions that are similar to the laboratory conditions.

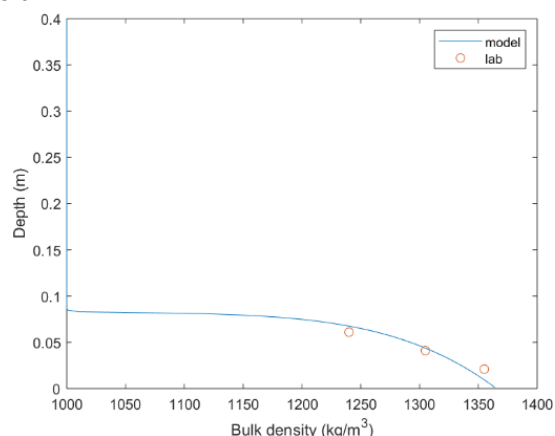


Fig D-1. Comparison between model results as obtained with C1 consolidation settings for C1 laboratory initial conditions, and laboratory measurements performed at the C1 column

D.3.2 Input to consolidation model II: field measurements

Though not conducted by Deltares, this section provides an overview of an important set of field measurements that were considered in this study. A hydrodynamic conceptual picture of the field situation is necessary in order to run the consolidation model for field conditions. This conceptual picture is built up from field measurements performed and provided by Biomanco, in particular by Alejandra Gijon Mancheno. Measurements were taken during monsoon season in 2018.

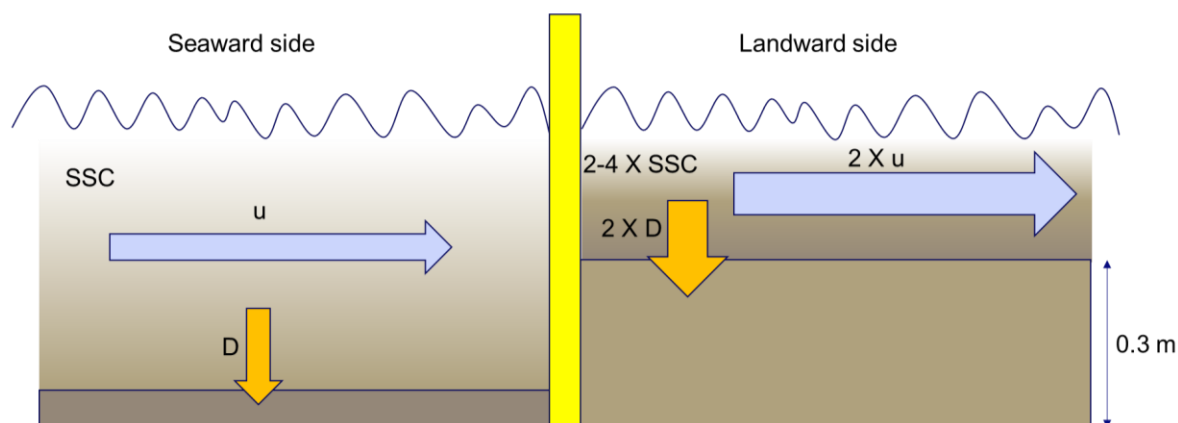


Fig D-2. Conceptual picture of the field situation. The yellow bar in the middle of the picture represents a permeable structure. The seaward and the landward side are defined by their current velocity (u), deposition flux (D), and their suspended sediment concentration (SSC).

Fig D-1 shows the conceptual picture as defined for our study site in the context of the consolidation study. The yellow bar in the middle of the picture represents a permeable structure. The seaward and the landward side are defined by their current velocity (u), deposition flux (D), and their suspended sediment concentration (SSC). The water depth in the landward side of the permeable structure is 0.3 m shallower, resulting previous sedimentation of mud. This is therefore a conceptual picture based in the current situation in the field (and not just after installing the structures). The size of the arrows and the coefficients in **Error! Reference source not found.** are an indication of the magnitude of the defining variables relative to the seaward size of the permeable structure. Note that, for example, when a coefficient 2 is given it does not mean that the variable in question is always a factor 2 larger than the reference, but just larger than the reference and up to a maximum of approximately a factor 2. For detailed information over the hydrodynamic parameters, the reader is referred to reports from the Biomanco project, owner and author of the data.

Here, an indication of the range in which the parameters varied is given bellow. All data was acquired at the so-called Bogorame measuring location, and over three days during November 2018.

Seaward side of the permeable structure:

- SSC: it was fairly stable over the 3 day measuring period, and varied mostly between 0.2 g/l and 0.3 g/l.
- u : it varied roughly between 0.005 m/s and -0.005 m/s.
- D : was defined by a characteristic gross deposition flux of 19 kg/m²/day (equivalent to 150 g of sediment at the sediment trap of Biomanco over 1 day, which was located at the seaward side, but still next to a permeable structure).
- The water depth was approximately 1 m, plus minus the tidal range.

Landward side of the permeable structure:

- SSC: in general ranging between 0.4 and 0.5 g/l, but with frequent peaks in the 1 g/l to 2 g/l range.
- u : it varied roughly between 0.005 m/s and -0.005 m/s as well, but this time with frequent peaks between 0.01 m/s and -0.01 m/s (which was not the case for the seaward side).
- D : A characteristic gross deposition flux of 38 kg/m²/day (equivalent to 300 g of sediment at the sediment trap of Biomanco over 1 day, which was located next to a permeable structure).
- The water depth was approximately 0.7 m, plus minus the tidal range.

Note that model results will be given only for the landward hydrodynamics (or under no hydrodynamics at all, see section 2.3.). Yet the conceptual picture provided includes the seaward situation, as the

landward hydrodynamics are defined here as a function of the seaward conditions (e.g. if the suspended sediment concentration at the seaward side is defined as SSC, this at the landward side is defined as 2-4 X SSC). The latter is relevant for placing the results in the context of the overall project aim, but not for the direct interpretation of the consolidation model results per se.

D.3.3 In-situ bulk density profiles

Fig D-3 shows multiple in-situ bulk density profiles, both at the landward (letter D; left panel) and seaward (letter E; right panel) side of the permeable structures. All profiles were measured at the same instant in time, but at different locations. The continuous blue line in both panels of represents the average of all the individual profiles shown in each of the panels. The measurements displayed in the figure were all obtained during a field campaign in November 2019, and as indicated in the methodology section more information about them can be found in Koster (2019).

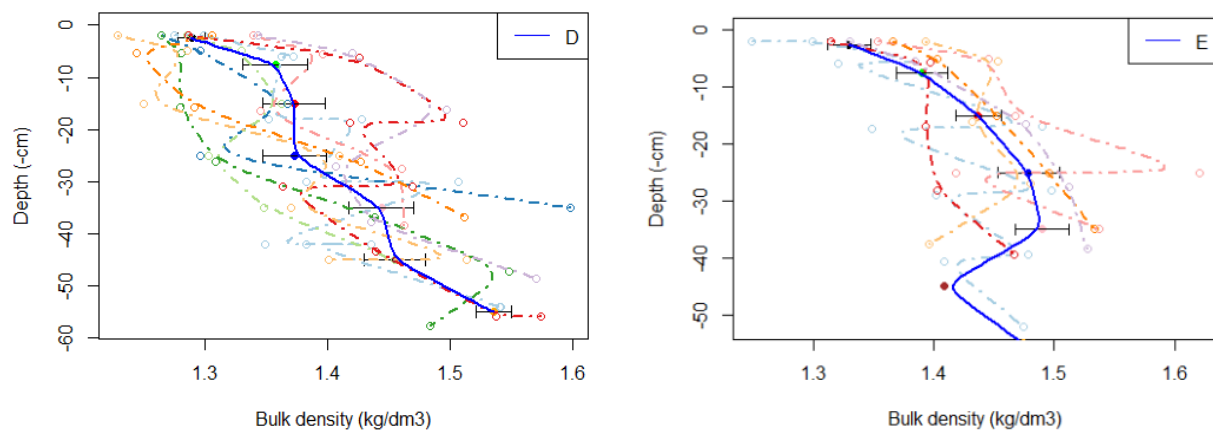


Fig D-3. Multiple in-situ bulk density profiles. The left panel contains profiles measured in the landward side of the structures. The right panel shows profiles measured in the seaward side of the structures.

The most important difference between the landward (letter D; left panel) and the seaward (letter E; right panel) bulk densities is that the landward side exhibits a less consolidated upper 30 to 40 cm of bed. By looking at the blue average profiles, it can be seen that for the landward situation (letter D; left panel) 1400 kg/m³ is reached at approximately 30 cm depth. For the seaward situation (letter E; right panel), 1400 kg/m³ is reached at less than 10 cm depth. By looking at the individual measurements (the dots conforming all other profiles), it can be seen that in the landward side (letter D; left panel) there are numerous points smaller than 1400 kg/m³ over the upper 40 cm of depth. For the seaward situation there are a lot less points smaller than 1400 kg/m³, and only over the uppermost 20 cm of bed.

D.3.4 Model results

Once developed and calibrated, the model was used to explore what the field observations by Biomanco may mean in terms of consolidation behavior. To this end, two configurations were modelled: an initial deposition event of 38 kg/m² (deposited at the gelling concentration of 90 g/l, as determined by “Soil Properties Demak”) which consolidated in the absence of hydrodynamics, and an initial deposition event of 38 kg/m² which consolidated under the measured hydrodynamics at the landward side of the structure. Note that 38 kg/m² is the characteristic daily gross deposition rate as measured by Biomanco and introduced in section 2.2. The conditions modeled in this simulation are not realistic, as not all the sediment (corresponding to the gross daily deposition flux) will become available for consolidation at once. Nevertheless, this initial condition is reasonably close to reality and will still give us an indication of the time and length scales involved.

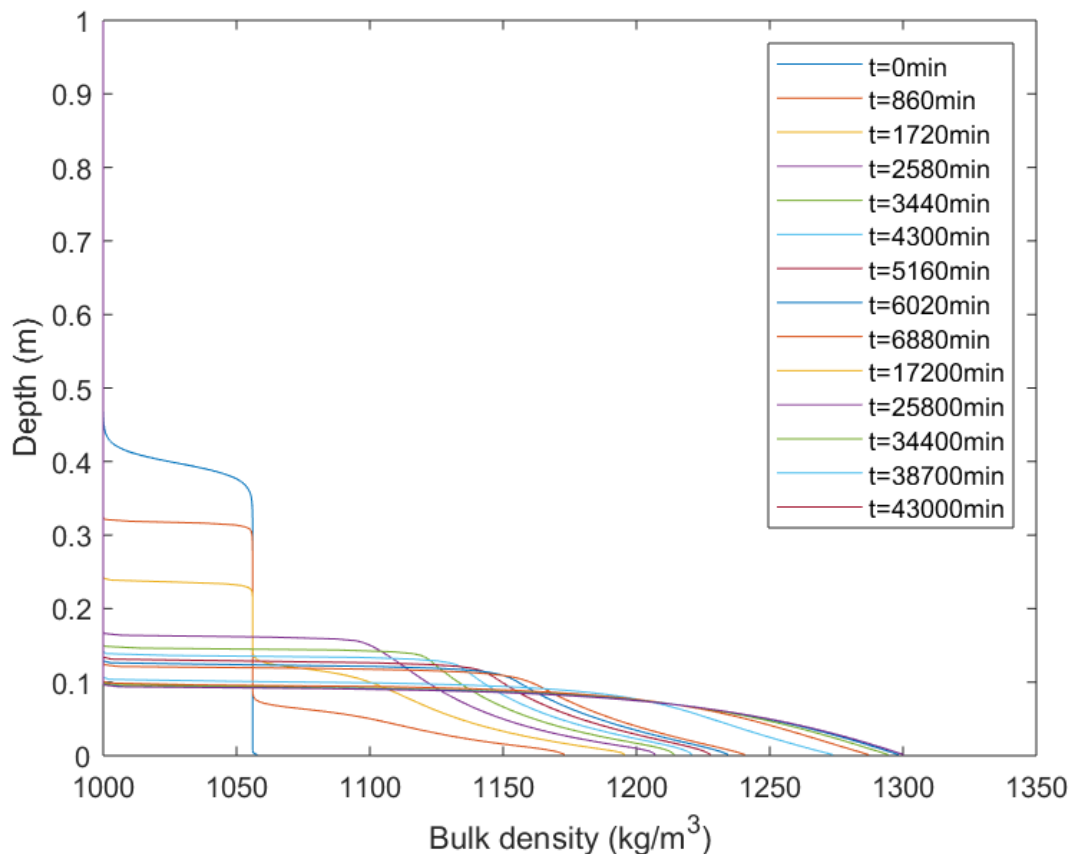


Fig D-4. Bulk density as a function of depth for a initial sediment layer of 38 kg/m^2 at a concentration of $c=90 \text{ g/l}$, which consolidates in the absence of hydrodynamics. Multiple bulk density profiles are plotted in different colors, with the legend representing the time in minutes at which each of the bulk density profiles is produced by the model. The first 10 profiles are plotted with a frequency of 860 min (14 hours approx.). Later, bulk density profiles are plotted with a frequency of 6 days.

Fig D-4 shows the model output for an initially deposited layer of 38 kg/m^2 (at the gelling concentration of 90 g/l) that consolidates under the absence of hydrodynamics. Multiple bulk density profiles are plotted in different colors, with the legend representing the time in minutes at which each of the bulk density profiles is produced by the model. The first 10 profiles are plotted with a frequency of 860 min (14 hours approx.). Later, bulk density profiles are plotted with a frequency of 6 days. In less than 2 days (2580 min), the initially high concentrated sediment suspension of 90 g/l over 40 cm have turned into a 15 cm soft bed whose densities range between 1100 and 1200 kg/m^3 . The soft bed continues to gradually dewater and compact over the course of days, reaching a more compact bed of 10 cm which bulk densities ranging from 1200 to 1280 kg/m^3 in approximately 20 days (17200 min). The final consolidated bed of still roughly 10 cm but with bulk densities reaching 1300 kg/m^3 is reached after 50 days (43000 min).

A 15 cm soft bed occurred, 2 days after deposition took place and consolidation started. These rates of 7.5 cm/day of soft bed accumulation are a lot higher than observations in the landward side of structures (or elsewhere). This suggests that the input of sediment is not a limiting factor (38 kg/m^2 was in fact measured in the field over one day), not at least during the monsoon (when 38 kg/m^2 was measured). It can therefore be expected that the realized sedimentation reflects the stability of the sediment material, not limitations on the input of sediments. Moreover, only 2 days are needed to accumulate 15 cm of a soft bed. There must be ample opportunities in the field to have such sedimentation events.

Thus, the build-up of sediment behind the permeable structures essentially depends on how strong this accumulated sediment is against erosive forces.

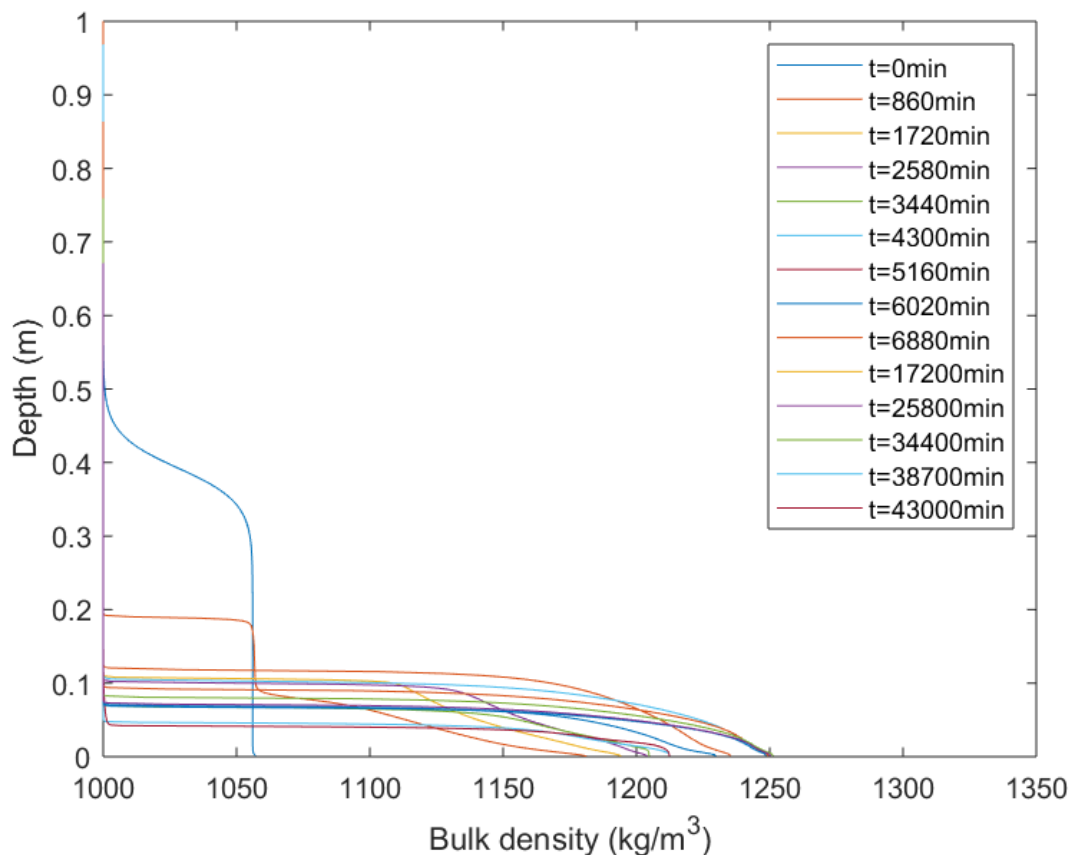


Fig D-5. Bulk density as a function of depth for a initial sediment layer of 38 kg/m^2 at a concentration of $c=90 \text{ g/l}$, which consolidates under the landward hydrodynamics. Multiple bulk density profiles are plotted in different colors, with the legend representing the time in minutes at which each of the bulk density profiles is produced by the model. The first 10 profiles are plotted with a frequency of 860 min (14 hours approx.). Later, bulk density profiles are plotted with a frequency of 6 days.

Fig D-5 shows the model output for an initially deposited layer of 38 kg/m^2 (at the gelling concentration of 90 g/l) that consolidates under the hydrodynamics characteristic of the landward side of a structure. The same convention as in Fig D-5 is applied for the frequency in which bulk density profiles are calculated by the model. These results indicate that hydrodynamics have a significant effect in determining the bulk density, and most probably also the strength. Under realistic average conditions the bed does not consolidate to the same density as in the absence of hydrodynamics (a maximum of 1250 kg/m^3 against the 1300 kg/m^3 obtained with no hydrodynamics). The equilibrium deposited thickness also turns smaller under the influence of hydrodynamics and decreases from 10 cm to 7 cm (30% smaller). Small stirrings of the bed are limiting the consolidation in the field. Probably such stirring would become less important for deeper layers, so that large sedimentation events may be really important in providing a protective layer allowing proper consolidation of the deeper sediment layers. This could be an explanation why initial sedimentation behind the dams is important and effective, but later on very little sedimentation is seen: there is a self-reinforcing aspect to sedimentation.

Furthermore, field measurements executed by the Deltares team during the numerous field campaigns indicated that bulk densities smaller than 1300 kg/m^3 had virtually no strength (our hand vane could not measure it as the bed was too weak). Therefore, the average hydrodynamic conditions lead to a weak bed that remains subject to erosion for prolonged periods of time and that may, eventually lead to little or no net sedimentation in the long run.

Net sedimentation may depend on exceptionally quiet conditions for prolonged periods of time, or on the fast sedimentation of a thick layer of sediment that may be capable of shielding the underlying layers

from hydrodynamic stirring. In any case, the relation between bulk density and strength of the bed is important and should be studied in more detail², as it will be key to understanding the net sedimentation processes.

D.4 Discussion – conclusion

A consolidation model was successfully developed and calibrated via a combination of laboratory experiments and field measurements. The model is capable of reproducing laboratory results, in particular these that realized the sediment bulk densities as observed in the field. This model was later used to perform a consolidation study, which revealed several important aspects of the consolidation dynamics in the study area.

First, modeling consolidation under the absence of hydrodynamics for a deposited layer equal to the gross deposition flux as measured in the field, resulted in the sedimentation of roughly 15 cm of soft bed in two days, which is not consistent with our field observations. This suggests that sediment supply is not a limiting factor for sedimentation, not at least during the monsoon period over which the deposition flux was measured³. Moreover, initial consolidation is fast, indicating that consolidation time scales should also not have a major role in determining net sedimentation. There should be ample opportunities in the field to have such sedimentation events, with the strength that the accumulated sediment can attain being of more relative importance for the final net sedimentation.

The model was later run for the same deposited layer (still equal to the gross deposition flux as measured in the field) but this time to consolidate under the measured field hydrodynamics (these of the landward side). In this case the model predicted a thinner, less dense, and most likely weaker layer as a result of consolidation. Average hydrodynamic conditions can therefore limit consolidation of the bed. We hypothesize that this effect is smaller at deeper sediment layers, suggesting a self-reinforcing aspect to sedimentation (the lower layers in thick deposited layers will be better protected from hydrodynamics, hence consolidating more efficiently). The weaker sediment layer resulting from consolidation under average hydrodynamics will be more susceptible of being eroded at potential future eroding events, eventually resulting in very little net or no sedimentation. Net sedimentation may depend on quiet hydrodynamic conditions for prolonged periods of time, or on the fast deposition of a thick layer of sediment that may be capable of protecting the underlying layers from the stirring effect of hydrodynamics.

² As mentioned, Deltares did include shear strength measurements in one of their field campaigns, but the amount of data collected was not relevant enough to draw conclusions, apart from the already mentioned fact that sediment with a bulk density smaller than 1300 kg/m³ did not produce any reading in our hand vane

³ Note that the gross deposition flux was measured next to a permeable structure.

D.5 References

- Gibson, R. E. (1958). The progress of consolidation in a clay layer increasing in thickness with time. *Geotechnique*, 8(4), 171-182.
- Gijón Mancheño, A. (2020). Mangrove restoration using brushwood structures. PhD thesis of Delft University of Technology.
- Koster, Jip (2019). The effect of permeable structures on spatial sediment dynamics and mangrove reoccurrence, MSc thesis of WUR and Deltares
- Merckelbach, L. M., & Kranenburg, C. (2004). Determining effective stress and permeability equations for soft mud from simple laboratory experiments. *Géotechnique* 54 (9), 581–591.
- Winterwerp, J. C., & Van Kesteren, W. G. (2004). *Introduction to the physics of cohesive sediment dynamics in the marine environment*. Elsevier.
- Winterwerp, J. C. (2006). Stratification effects by fine suspended sediment at low, medium, and very high concentrations. *Journal of Geophysical Research: Oceans*, 111(C5).
- Winterwerp, J. C. (2002). On the flocculation and settling velocity of estuarine mud. *Continental shelf research*, 22(9), 1339-1360.

Deltares is an independent institute for applied research in the field of water and subsurface. Throughout the world, we work on smart solutions for people, environment and society.

Deltares

www.deltares.nl